Manuscript Details

Manuscript number	SAB_2017_131_R1
Title	Reliability of portable X Rays Fluorescence for the chemical characterization of ancient corroded copper-tin alloys
Article type	Research Paper

Abstract

This paper examines the effect of different corrosion patinas on the chemical composition of copper-tin alloys detected by portable X-ray Fluorescence Spectroscopy (pXRF). Specimens of Cu88Sn12 alloy with a composition close to that of ancient Egyptian copper-based alloys were corroded in three different aqueous solutions containing aggressive anions that can be found in Egyptian soil, for a maximum time of three months. After each sample was extracted, the elemental composition was determined with pXRF and the surface morphology and cross-sections were observed by metallographic microscopy to measure the thickness of the corrosion patinas. The cross-section of selected samples was analysed with Scanning Electron Microscopy equipped with Energy Dispersive X-ray Spectrometer (SEM-EDS). During the corrosion evolution of the copper alloy in the corrosive solutions of chlorides, decuprification phenomena made XRF data less accurate due to the development and thickening of Sn compounds (oxides or chlorides). Another problem encountered in the detection of the chemical composition of the Cu88Sn12 alloy was the bronze disease that strongly increased the corrosion process leading to the formation of an outer layer of atacamite and paratacamite, reaching a thickness of 150 μm. Conversely, during the corrosion process of the samples immersed in a sulphate solution, no changes in the initial composition of the Cu88Sn12 alloy were observed. The attenuation effect of the Sn concentration, by the thickness of green/dark green patinas with a high chloride content was observed on two Egyptian toilet spoons from the Museo Egizio (Turin) using pXRF. Following comparison of the chemical compositions in different corrosion patinas, it emerged that the red and grey patinas did not suffer the attenuation effects and, at these points of analysis, a reliable chemical characterisation of the alloy was obtained.

Keywords	Portable X-ray Fluorescence; Copper alloy; Corrosion; Bronze; ancient Egypt

Corresponding Author	Angelo Agostino
Corresponding Author's Institution	Università di Torino
Order of Authors	Simone Robotti, Paola Rizzi, CHIARA SOFFRITTI, Gian Luca Garagnani, Christian Greco, Matilde Borla, Federica Facchetti, Lorenza Operti, Angelo Agostino

Submission Files Included in this PDF

File Name [File Type]

Cover_letter_Journal of Spect Acta B.docx [Cover Letter]

171004 Referees answers SA_B_final.docx [Response to Reviewers]

171004_highlight file.docx [Highlights]

Graphical Abstract.tif [Graphical Abstract]

171004_Egyptian alloys_final.docx [Manuscript File]

Fig.2.tif [Figure]

Fig.3.tif [Figure]

Fig5.tif [Figure]

Fig7.tif [Figure]

Fig8.tif [Figure]

Fig9.tif [Figure]

Fig10.jpg [Figure]

Figures Captions.docx [Figure]

Fig.1.tif [Figure]

Fig.4.tif [Figure]

Fig6.tif [Figure]

FigS4_1_XRD_A_60.tif [Figure]

FigS4_2_XRD_B_60.tif [Figure]

FigS4_3_XRD_C_60.tif [Figure]

171004_Tables.docx [Table]

To view all the submission files, including those not included in the PDF, click on the manuscript title on your EVISE Homepage, then click 'Download zip file'.

Università degli Studi di Torino
Dipartimento di Chimica
Via P. Giuria, 7 10125 Torino Italy

chimica

dr. Angelo AGOSTINO
phone: +39 0116707585
fax: +39 0112367585
e-mail: angelo.agostino@unito.it

Torino, 10/04/2017

Dear Editor,

please find enclosed our communication entitled:

"**Reliability of pXRF for the chemical characterisation of ancient copper-tin alloys**",

by Simone Robotti[1,2], Paola Rizzi[1], Chiara Soffritti[2], Gian Luca Garagnani[2], Christian Greco[3], Federica Facchetti[3], Matilde Borla[4], Lorenza Operti[1,5], Angelo Agostino[1,5]*

(1) Dipartimento di Chimica, Università di Torino, Via Giuria 7, 10125 - Torino, Italy
(2) Dipartimento di Ingegneria, Università di Ferrara, Via Saragat 1,44122 - Ferrara, Italy
(3) Fondazione Museo delle Antichità Egizie di Torino, Via Accademia delle Scienze, 6, 10123 Torino, Italy
(4) Soprintendenza Archeologia, Belle Arti e Paesaggio per la città metropolitana di Torino, Piazza San Giovanni, 2 - 10122 Torino, Italy
(5) CRISDI (Interdepartmental Centre for Crystallography), Via Giuria 7, Torino, Italy

that we submit for publication in *Spectrochimica Acta B* as research paper.

We believe that this manuscript is suitable for the high level of *Spectrochimica Acta B* as our findings constitute a significant advance in both the X ray spectrometry research area and Cultural Heritage field, because of the following reasons:

1- the subject of the investigation, concerning the application of portable XRF on patinated metallic surfaces could be an improvement of the possibilities on quantitative approach of this technique in museum application field;
2- the completeness of the study, based on a wide laboratory experimental part, give the requested robustness to the acquired and discussed data;
3- the laboratory and in situ approach conjugated with the discussion of the patinated layers influence on XRF analysis (in situ and ex situ) extend the possible quantitative application of this portable technique as highlighted in the results obtained to the Museo Egizio in Turin.

In our opinion, the mentioned results are of clear interest for the scientific community.

Thank you for your attention

Best regards,

Angelo Agostino

*corresponding author
Angelo Agostino
Dipartimento di Chimica
via P. Giuria, 7
10125 – Torino, IT
phone: +39 0116707585
e-mail: angelo.agostino@unito.it

Dear Margaretha de Loos-Vollebregt,

in the following pages are reported all the answers and the variation related to the comments of all the referees about the scientific article:

"*Reliability of pXRF for the chemical characterisation of ancient copper-tin alloys*" written by Simone Robotti, Paola Rizzi, Chiara Soffritti, Gian Luca Garagnani, Christian Greco, Federica Facchetti, Matilde Borla, Lorenza Operti and, Angelo Agostino

- **Answers to Editor comments**

1. Position your work clearly with respect to studies already published and focus on what is new.

This work is based on the possibility to extend the use of X-ray fluorescence equipments in a museum environment in order to analyze metal alloys in presence of patinas (or thin corrosion layers) by means of a strictly controlled quantification process.

This approach aims to increase the reliability of portable XRF, evaluating and stressing its potential given that on one side it as a tool available to both scientists and conservators and on the other side, taking into account the problematics of its application to the field of Egyptian artifacts.

All these observations have been included in the text.

2. Use full wording for pXRF in the title.

According with the editor's suggestions, the title and all the related text have been modified.

3. Define uncertainties in the tables and and add definition of error bars in the figure captions where appropriate.

The explanation of the error bars meaning for figures 5 and 8 have been inserted in the captions.

4. Please check the figures. Provide missing axis titles and units (Figs. 1b, 4b, 6b).

As observed, all the missed axis titles have been corrected.

5. Highlights. Please note that there should be a maximum of 85 characters, including spaces, per highlight. Only the core results of the paper should be covered.

As suggested the highlights file was corrected.

6. For publication of supplementary content, please check the Guide for Authors and recent issues of SAB. In the text please refer to figures in the appendix as Fig. S1 (Appendix), Table S1 (Appendix), etc.. After the Acknowledgement the following text should be inserted 'Appendix A. Supplementary data' and 'Supplementary data to this article can be found online at doi:...'. The reader can access the data online with the article. Please upload the appendix as separate file. Add the title and authors at the first page. Position the figure captions below the corresponding figures.

A new chapter named Appendix A has been inserted in the article after the Acknowledgements chapter.

7. Please check and correct language. Ask help from a native English colleague or ask professional advice.

Done.

- **Answers to #1 referee comments**

Very interesting paper, well done and well written. It can also be used as a work-guide for methodology about multi-technique application on cultural heritage samples . I recommend to accept it without substantial changes.

There are no replies to the present comment but indeed an acknowledgment to the understanding of the different approach introduced by our paper.

- **Answers to #2 referee comments**

1. Title: be more precise and mention corrosion explicitly

The title has been modified as suggested.

2. Materials and methods:

What is the metal resp. patina METHOD? Do you mean the measuring conditions? Did you optimize the conditions or is it a feature of the Thermo Niton spectrometer?

The quantification process consists of a complex approach including the comparison of the Thermo Niton built-in software with some close and open source softwares as WinAxil and PyMCA. In addition, a homemade software has been used to check the contribution of the corrosion layers.

Anyhow, the topic of this work is not the evaluation of software simulations for what refers to the production of better or worst quantitative results about the corrosion layer. Instead, this work concerns the reliability of pXRF method within a controlled experimental approach where the thickness of the corrosion layers are directly measured and quantified by SEM analysis. The goal was to underline the inefficacy of the pXRF method or, better, until the method returns reliable data in quantifying a corroded metal alloy.

The difference between metal and patina methods is mainly based on a different way of the algorithm in considering the scattering curves (elastic and inelastic) for what concerns the quantification of the dark matrix. In the case of the patina algorithm, the contribution of the light elements to the final metal alloy composition takes into account the not measurable elements, i.e. the dark matrix. In the metal algorithm approach, instead, only the metal elements are quantified and the results are normalized. It has been observed (see appendix for the supplementary information) that the comparison of the scattering influence shows that there is not particular difference (all inside the 2sigma error bars) between the two algorithms if the patina contribution is excluded.

3. 3mm spot size is not really small

This statement of course has to be considered within the context. In this method a millimetric spot size allows reaching a certain statistic, which is determinant for our scopes and is obviously not comparable to other microscopic methodologies. Moreover, the small size term is referred to the 3 millimeter spot instead of the 8 millimeter available in the NITON experimental setup.

4. How did you get quantitative results? Which method is used? Your homemade software did what?

Please refers to the answer in point 2.

5. This should be explained in S1. For me it is not clear what you have done. Did you just make a variation of the measuring times or did you really tried different quantification methods?

The supplementary information provided in S1 is given for transparency on the data production. In this section, the analyses realized on certified reference materials with different peculiarities (heavy and light matrices) have been reported, and different times and algorithms were used to evaluate the uncertainly introduced by the methods or boundary conditions.

6. In S1 and other parts of the paper you suddenly talk about the metal /patina ALGORITHM. Please state clear what you mean by this.

Please refers to the answer in point 3.

7. Please rewrite the method section and make clear what is your work, what is new and what is just application of in-built functions.

As suggested by referee #2, the method section was revised adding information about the algorithms used.

8. The results section describes very well your interesting insights. Anyhow, maybe it would be easier for the reader to visualize your results and not to give this big tables. They can move to the supplement.

In accord with the referee suggestions the data tables for the different solutions has been moved in the supplementary information. Only the result discussion is reported on the paper.

9. In the conclusion section I miss a part, which compares your method to others, which has been used successfully to correct for corrosion effects.

e.g. C. Bottaini et al , Spectrochimica Acta Part B: Atomic Spectroscopy, Volume 103, 2015, Pages 9-13,

The authors are well aware of Bottaini and Schiavon works. In the present case, however, the focus of the work is not related to the simulation of the influence of the patina thickness on the spectrum profile (and consequently on the elements quantification) but, with an opposite process, to define, analyzing the spectrum collected on the patinated samples, which is the threshold thickness allowing to obtain a reliable information on the bulk composition.

The statistical approach is the basis of this method: the millimetric area of analysis and the observation of different types of patinas allows have provided a good quantitative estimation of the bulk composition in a corroded bronze alloy.

For this reason, the papers cited by the referee, obviously inherent to the general topic of corroded alloys but focusing on a different perspective, are not in line with the subject of this research and thus they were not cited or included in the discussion.

Good Luck!

- **Answers to #3 referee comments**

The ms reports a study on the effects of the presence of corrosion patinas experimentally produced on test Cu bronze samples of known composition (Cu88-Sn12), regarded as typical of Egyptian bronzes, on the reliability of quantitative data obtained by p-XRF. The topic is highly relevant in the field and the experimental data presented is welcomed. In this respect, I believe that the paper is worth of publication, provided that the authors address satisfactorily the following comments:

1) Could the authors provide a better explanation why they have specifically chosen the adopted protocol for accelerated corrosion test (i.e. immersion on solutions mimicking Egyptians soil conditions) rather than other techniques.

The discussion developed in this article focuses on the simulation of certain types of corrosion phenomena occurring on bronze alloys, specifically related to ancient Egyptian bronzes. The applied protocol provides better and more repeatable results in a more reasonable amount of time. The use of a climatic room and the immersion of the samples in soil mixtures, in our opinion, would have been too much time expensive. Furthermore, the use of ground mixtures cannot give a simplified situation useful for the modeling protocol.

2) In the introduction, additional recently published work addressing the same analytical problem of the reliability of using p-XRF for the quantitative analysis of ancient bronzes with corrosion patinas and/or measuring patinas thicknesses on multilayered materials using alternative protocols should be mentioned including for example:

- Schiavon et al. An Energy-Dispersive X-Ray Fluorescence Spectrometry and Monte Carlo simulation study of Iron-Age Nuragic small bronzes ("Navicelle") from Sardinia, Italy Spectrochimica Acta Part B 123 (2016) 42–46

- C. Bottaini et al., Energy dispersive X-ray fluorescence spectroscopy/Monte Carlo simulation approach for the non-destructive analysis of corrosion patina-bearing alloys in archaeological bronzes: the case of the bowl from the Fareleira 3 site (Vidigueira, South Portugal), Spectrochim. Acta B 103-104 (2015) 9–13.

Cesareo et al. 2013 Multilayered samples reconstructed by measuring Ka/Kb or La/Lb X-ray intensity ratios by EDXRF. Nuclear Instruments and Methods in Physics Research B 312 (2013) 15–22

As already reported in point 9 of the answers to referee #2 section, the authors are aware of the upcited papers. In these works, the simulation method, absolutely efficient and reliable, is focused on the developing of a software method able to predict the thickness in relationship to the composition of a generic corrosion layer. In a real case, however , the thickness and layer composition (here considering the dark matrix) are unknown. In the present paper the discussion introduces a method willing to understand if it is possible or not to obtain reliable information on the metal alloy considering the presence of a corrosion patina.

3) I would invite the authors to double check the English language in the whole text. A few examples of misspellings and errors are marked in the attached ms.

Thank you to the referee for this annotation, we checked the English language as requested.

4) Considering the inherent inhomogeneity of Cu-alloys and of their corrosion patinas which can be seen also in fig. 1, could the authors indicate how many spots of XRF analysis were carried out per each sample?

Usually, seven points of analysis have been used.

The inhomogeneity of the samples is a focus point that will subject of a following publication. In that work we are going to address an unexpected results obtained applying the up-cited method to the analysis of corroded metal alloys. Indeed, our empirical results indicate that the statistical distribution of the quantitative composition of the bulk metal appears to be uncorrelated with the different degradation phases observed on the corroded surface.

5) in Solution B, sulphuric acid was added to obtain a pH=3. Do the authors really believe that these conditions may reflect a real situation in Egyptian soils?

The analyses realized on Egyptian bronzes show that Brochantite is one of the most relevant phases of the corrosion layer (Ghoniem 2011, 2016). In order to reproduce this corrosion product in laboratory conditions (and in reasonable time) the authors decided to use the receipt indicated by Hayez et al., 2005 and Leyssens et al., 2006. In these papers, the simulation of the conditions of the Egyptian soil applied to produce Brochantite implies the use of sulfuric acid to regulate the pH and the anionic content of sulphates.

6) More information should be added (maube as supplementary file) on the Patina and Metal algoritms

Following the referee suggestion, a dedicated part was included in the materials and method section. Please refer to point 2 in the answers to referee #2 section.

7) More information should be added on the estimated threshold values of the patinas thickness that the authors believes are critical for the reliability of the XRF data to be considered acceptable.

On the basis of the obtained results, the threshold values can be estimated around 100 um. This threshold is critical for solution C (with chlorines) and A (with carbonates and chlorates) as the quantitative information obtained using XRF is no more representative of the alloy if applied on samples with a thicker patina. On the other hand, for what concerns solution B, the reliability of the quantitative result is maintained also for patinas produced after 90 days of investigation resulting in more than 100um thick patinas. Therefore, in order to find the threshold for the solution B a more extended monitoring period is needed, in any case indicating a threshold thickness over 100 um.

8) XRD diagrams should be provided.

XRD patterns of the three used solutions were included in the supporting information (S4).

Please see also see comments in attached, annotated ms

Highlights file

- Ancient Egyptian alloys, their evolution their corrosion has been discussed.
- A laboratory study on the corrosion phenomena was investigated on similar alloys.
- Potentialities and limits of quantitative pXRF on patinated alloys were exposed.
- A *casus studi*, realized to the Egyptian Museum of Turin, was realised.

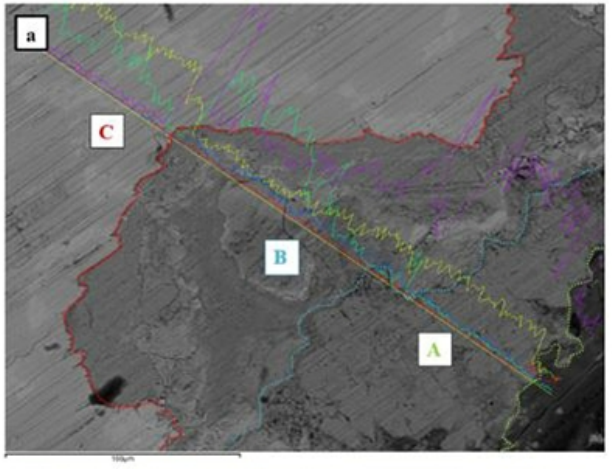
a
C
B
A

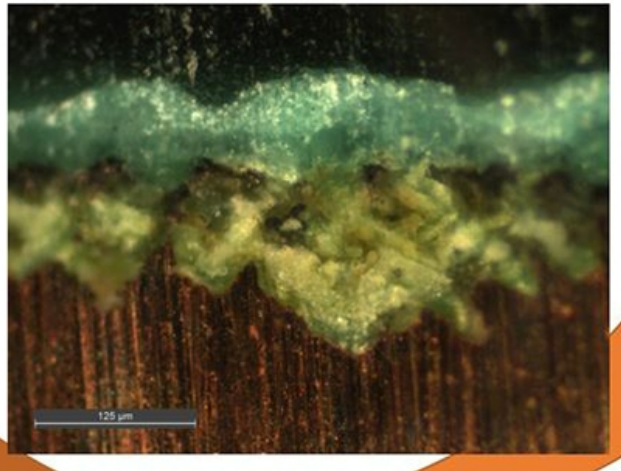
125 µm

Reliability of portable X Rays Fluorescence for the chemical characterisation of ancient corroded copper-tin alloys

Simone Robotti[1,2], Paola Rizzi[1], Chiara Soffritti[2], Gian Luca Garagnani[2], Christian Greco[3], Federica Facchetti[3], Matilde Borla[4], Lorenza Operti[1,5], Angelo Agostino[1,5]

(1) Dipartimento di Chimica, Università di Torino, Via Giuria 7, 10125 - Torino, Italy
(2) Dipartimento di Ingegneria, Università di Ferrara, Via Saragat 1,44122 - Ferrara, Italy
(3) Fondazione Museo delle Antichità Egizie di Torino, Via Accademia delle Scienze, 6, 10123 Torino, Italy
(4) Soprintendenza Archeologia, Belle Arti e Paesaggio per la città metropolitana di Torino, Piazza San Giovanni, 2 - 10122 Torino, Italy
(5) CRISDI (Interdepartmental Centre for Crystallography), Via Giuria 7, Torino, Italy

Abstract

This paper examines the effect of different corrosion patinas on the chemical composition of copper-tin alloys detected by portable X-ray Fluorescence Spectroscopy (pXRF). Specimens of $Cu_{88}Sn_{12}$ alloy with a composition close to that of ancient Egyptian copper-based alloys were corroded in three different aqueous solutions containing aggressive anions that can be found in Egyptian soil, for a maximum time of three months. After each sample was extracted, the elemental composition was determined with pXRF and the surface morphology and cross-sections were observed by metallographic microscopy to measure the thickness of the corrosion patinas. The cross-section of selected samples was analysed with Scanning Electron Microscopy equipped with Energy Dispersive X-ray Spectrometer (SEM-EDS). During the corrosion evolution of the copper alloy in the corrosive solutions of chlorides, decuprification phenomena made XRF data less accurate due to the development and thickening of Sn compounds (oxides or chlorides). Another problem encountered in the detection of the chemical composition of the $Cu_{88}Sn_{12}$ alloy was the bronze disease that strongly increased the corrosion process leading to the formation of an outer layer of atacamite and paratacamite, reaching a thickness of 150 μm. Conversely, during the corrosion process of the samples immersed in a sulphate solution, no changes in the initial composition of the $Cu_{88}Sn_{12}$ alloy were observed. The attenuation effect of the Sn concentration, by the thickness of green/dark green patinas with a high chloride content was observed on two Egyptian toilet spoons from the Museo Egizio (Turin) using pXRF. Following comparison of the chemical compositions in different corrosion patinas, it emerged that the red and grey patinas did not suffer the attenuation effects and, at these points of analysis, a reliable chemical characterisation of the alloy was obtained.

Keywords

Portable X-ray Fluorescence; Copper alloy; Corrosion; Bronze; ancient Egypt.

1. Introduction

Due to different possible interactions between ancient metallic artefacts and various environments, as well as the different preservation conditions, the corrosion processes of metallic materials remain a complex topic that is still under investigation. Moreover, the use of portable X-ray Fluorescence (pXRF) devices to measure the elemental composition of bulk and corrosion layers of copper alloys [1-7], brings into question the reliability of the composition determined on metallic materials sometimes covered with thick patina layers, the composition of which can differ from the original composition of the alloy. Therefore, even though XRF Spectroscopy has the potential to provide precise and fast results, allowing for non-destructive measurements of archaeological applications to be made *in situ* [8], it is important to experimentally determine in which conditions corrosion layers can affect the elemental results in order to enable the measurements of reliable compositions.

Ancient bronze artefacts are subjected to corrosion processes that can involve the formation of corrosion patinas on their surface, besides possible inter-granular or intra-granular corrosion processes or galvanic electrochemical processes [9-11]. The corrosion processes of archaeological bronze were described by Robbiola et al. and classified as two types. In the type I corrosion process (or on "even" surfaces), the interaction of the artefacts with the soil leads to a galvanic corrosion with a selective dissolution of copper (i.e. decuprification) from the alloy and the consequent oxidation of the tin enriched layer with the formation of an outer Sn oxide rich layer, superimposed onto an internal layer composed of oxides and hydroxides in which the amount of Cu increases with respect to the outer layer. The type II corrosion process is due to a high dissolution rate of the alloy that involves the formation of three corrosion layers: (1) an outer zone of green Cu(II) compounds as malachite; (2) an intermediate red layer of cuprous oxide, often fragmented; (3) an internal layer characterised by high tin contents due to selective Cu dissolution associated with soil elements, O and Cl [12]. A recent study of the degradation phenomena of a bronze bowl of the Achaemenid Empire (559–330 BC) containing about 11% tin was analysed by pXRF, Raman spectroscopy and scanning electron microscopy equipped with energy dispersive spectroscopy (SEM-EDS). The results showed new corrosion structures: (1) a copper oxide (cuprite, tenorite)/tin oxide (cassiterite) layer; (2) a copper hydroxycarbonate (malachite, azurite) layer; (3) a copper(II) basic carbonate top layer, merged with other soil components [13].

The aim of this work is to study the corrosion process of a $Cu_{88}Sn_{12}$ alloy in different conditions in order to determine the corrosion products and to test the applicability of the pXRF when determining the chemical composition of the $Cu_{88}Sn_{12}$ alloy at different degrees of corrosion. Furthermore, the applicability of the method is proposed for the chemical characterisation of two toilet spoon copper based alloys C.6428 and P.624 from the Museo Egizio (Turin).

The $Cu_{88}Sn_{12}$ alloy was chosen due to its similar composition to the Egyptian bronzes of the New Kingdom (1550-1069 BC). The use of copper alloys started in Egypt from the middle Predynastic period [14,15]. From numerous analyses [16-24] it was concluded that arsenical copper alloys were used with an As content between 1 and 8% and Sn as a trace element (< 1 %) in the Old Kingdom (2700–2200 BC) and Middle Kingdom (1990–1630 BC). Bronze was used in the New Kingdom, where Sn usually varied between 2 and 16% [25]. During the Late Period, Ptolemaic and Roman Period, the Sn concentrations can exceed 20% [26].

This study aims to be a preliminary research in the systematic analysis of the frameworks of ancient copper alloys.

2. Materials and methods

$Cu_{88}Sn_{12}$ alloy was produced by casting the master alloy into three bar ingots and 28 samples (dimensions 2x2x1 cm) were obtained.

In order to perform the corrosion tests, three solutions were selected from the literature containing aggressive anions compatible with those obtained from the analysis carried out on Egyptian soils [27-30]. The solutions contained: 15.07 g of $(NH_4)_2CO_3$ and 10.02 g of NH_4Cl in 100 mL of de-ionised water (solution A); 0.6 g of $KClO_3$, 0.3 g of $CuSO_4 \cdot 5\ H_2O$ and 0.4 g of $N_2SO_4 \cdot 10\ H_2O$ in 100 mL of de-ionised water adjusted to pH=3 with H_2SO_4 (solution B); 10.02 g of $Cu(NO_3)_2 \cdot 3\ H_2O$ and 10.01 g of NaCl in 100 mL of de-ionised water (solution C).

The corrosion tests were conducted through immersion at room temperature in order to prevent evaporation of the solutions for different degrees of corrosion corresponding to predetermined times in the solutions (0, 1, 3, 7, 10, 15, 30, 60, 90 days (d)).

Each sample, previously grounded by abrasive silicon carbide papers of grade 180, 500, 1000, 2500, respectively, and then polished with diamond paste from 6 to 3 μm, were immersed in solutions in glass beakers closed with parafilm for 15 days, while the specimens from 30 days to 90 days were immersed in solutions in polyethylene bottles to avoid evaporation of the solution.

The specimens were removed from the solutions, rinsed with de-ionised water and left to dry. Subsequently, the $Cu_{88}Sn_{12}$ samples were observed with an optical microscope and were analysed by X-ray fluorescence (XRF), X-ray diffraction (XRD) and Scanning Electron microscopy (SEM). All XRF analyses were carried out by a Thermo Niton™ (USA) XL3t-900 EDXRF spectrometer, equipped with a silver target and a large-area silicon drift detector (SDD), with an energy resolution of 136 eV, calculated at 5.9 keV. The geometry used was 30°/30°, with a working distance of 2 mm orthogonal to the detector/source plane. The total analysis time was 120 s or 240 s, subdivided into four fractions (to optimise different energy ranges) respectively of 30 s or 60 s each for the "Patina" algorithm, and 60 s or 120 s subdivided into two fractions respectively of 30 s or 60 s each for the "Metals" algorithm. The different ranges were 50 keV at 50 μA with a Mo filter, 40 keV at 50 μA with a Fe/Al filter, 20 keV at 95 μA with a Cu filter and 8 keV at 95 μA with no filter, for the "Patina" method and 40 keV at 50 μA with a Fe/Al filter, 15 keV at 95 μA with a Fe filter and 6 keV at 95 μA for the "Metals" method. The spectra were processed using homemade software and the results were compared with the WinAxil CANBERRA commercial software. The instrument was kept in position by a custom stage allowing micrometric movements and all measurements to be conducted in air with a small spot (3 mm diameter). The "Patina" algorithm made it possible to detect the alloy and light elements (Cl, S, Si, Ca, K, Al, P), i.e. the chemical elements of the soil and corrosion products, while the "Metals" algorithm made it possible to detect only the elements present in the bulk. "Dark Matrix" (DM) is the concentration of the elements set that were not detected by XRF spectrometer (e.g. H, O, Na etc.).

The difference between "metal" and "patina" methods can be summarized on the difference between algorithms in considering the scattering curves (elastic and inelastic) in the quantification of the dark matrix. In the case of "patina" algorithm, we define the contribution of light elements in the variation of the metal alloy composition including the not measurable elements recoiled in the dark matrix. In

the “metal” algorithm approach, instead, just the metal elements are quantified and all the results are normalized.

In order to validate the quantitative analyses, measurements were conducted on certified composition standards. The Certified Standard Reference Materials (CRM): 31XB22E, 31XB17E, 31XMNB4E, 33XGM8F, 32XALB4G and 55XG900J3F, were produced by MBH Ltd. Each standard was analysed with both of the two quantitative algorithms and with different measurement times: 60 s (30 s for each energy range), 120 s (60 s for each energy range) and 180 s (90 s for each energy range) for the “Metals” algorithm; 12 0s (30 s for each energy range) and 240 s (60 s for each energy range) for the “Patina” algorithm.

The $Cu_{88}Sn_{12}$ alloy composition was calculated by the arithmetic mean of all the measurements carried out with the “Metals” algorithm (60 s for the measurement: 30 s for each energy range): Cu=86.6 ± 0.5 wt.%, Sn=11.9 ± 0.4 wt.%, Pb=0.97 ± 0.1 wt%, Ni=0.2 ± 0.02 wt.%, Zn=0.19 ± 0.04 wt.%, Sb=0.09 ± 0.02 wt.%.

XRF analyses of two copper-alloyed toilet spoons from the Museo Egizio were carried out by using the “Patina” algorithm (120 s) and the “Metals” algorithm (60 s) and the 3 mm spot analysis configuration.

Diffraction was carried out using a X’Pert PRO PW3050/60 PANalytical instrument equipped with a fast curved 1D silicon strip detector (X’celerator) operating at 40 kV and 30 mA with a Cu Kα radiation. The patterns analysis was obtained using a Bruker proprietary software (DIFFRACplus) and the Powder Diffraction File (PDF) database of The International Centre for Diffraction Data (ICDD). The patinas were analysed without any preparation (to preserve them) by inserting the specimens directly into the diffractometer.

Afterwards, the samples were sliced transversely, they were embedded in epoxy resin SpeciFix-40 (STUERS ApS – Denmark) and then polished for observation under a LEICA 2500M metallographic microscope equipped with an N PLAN (achromatic objectives up to 1000x) and LEICA DFC295 digital camera at 5M pixels, and polarization crystals. Observations were made of the sample surface, to detect the presence of corrosion products, and of the cross-section, to observe the stratigraphy of the corrosion patina and to measure its thickness. The corrosion products were characterised by a metallographic microscope with a dark field (DF) contrast system.

The samples were observed by Scanning Electron Microscopy using a JEOL JSM-IT300LV with Energy dispersion spectrometer Oxford INCA Energy 200 and PENTAFET detector (SATW). The working conditions were 15.0 kV and 300 pA and line analysis was carried out to determine that the cross section composition was recorded for 256 measuring points. The specimens embedded in epoxy resin were also polished on the back of the samples to guarantee electric conduction during the EDS measurements. SEM observations were made using both a backscatter (BED-C) and secondary electron (SED) detector.

3. Results and discussion

Initially, the portable instrumentation was calibrated by using CRM. Calibration was carried out by using different algorithms and focusing on the evaluation of analytical accuracy (more details are reported as supplementary information in appendix A).

3.1 Solution A

In the samples treated with the ammonium carbonate and ammonium chloride solution, the alteration observed at the surface was not significant up to 30 days. Only after 60 days there was a uniform light blue patinated layer detected by the metallographic microscope (XRD patterns are reported in Appendix A, figures S4_1).

The cross section SEM-EDS analysis carried out on the corrosion patina of sample A_90d revealed the presence of a tin reach corrosion layer that may support the hypothesis of the development of chloride or oxide Sn corrosion products that appears to be detached and fragmented due to the cross cutting and subsequent polishing of the samples. At the corrosion layer/bulk interface, EDS analysis revealed the presence of Cu, Sn and Cl, which was probably linked to a mixture of Cu chlorides and Sn oxides or chlorides (**Fig.1**). After 90 days, the thickness of the corrosion products was about 200 μm, including voids and not homogeneous areas.

Insert here Fig. 1

The XRD analysis, performed on the sample A_90d, confirms the presence of cassiterite (SnO_2) and paratacamite ($Cu_2(OH)_3Cl$) probably besides other amorphous corrosion products of Cu and Sn.

The Cu and Sn concentrations, determined by XRF analysis, up to 30 days, lay within the error bar of the initial measured composition, confirming the metallographic microscope observations and SEM-EDS analyses, where no remarkable morphological and compositional variations were observed. Moreover, between 60 days and 90 days, the Cu concentration determined by the XRF "Metals" algorithm decreased from 78 wt.% to 48 wt.% and the Sn concentration increased up to 43.3 wt.% in A_90d. The normalisation of the XRF data obtained with the "Patina" algorithm leading to Cu and Sn concentrations with values close to those obtained using the "Metals" algorithm (the complete data are reported in table S1 in Appendix A)

The corrosion model acting for samples immersed in solution A is depicted in **Fig 2**. It initially involves the development of a Cu depletion layer at the surface of the sample due to decuprification without the development of corrosion products up to 60 day of immersion in the corrosive solution (Phase 1). Subsequently, we can assume the development of Sn corrosion products (tin oxides or tin chlorides) and copper chloride corrosion products in A_90d (Phase 2). XRD analysis confirms the presence of tin oxide cassiterite and copper hydroxychloride paratacamite. In solution A, the XRF data become less accurate after 60 days due to the depletion of Cu that produces a rich Sn surface layer that leads to an increase in the Sn concentration. After 90 days, the composition measured by XRF is limited to the depletion layer and the corrosion products, due to their thickness that is higher than the volume interaction of the XRF. Therefore, the Cu concentration decreases strongly in A_90d due to the growth of the Sn corrosion layer and to the Cu depletion layer at the same time (**Fig.2**).

Insert here Fig. 2

3.2 Solution B

The second solution chosen is a mixture of potassium chloride, cupric sulphate pentahydrate and sodium sulphate decahydrate, which is more aggressive because of the addition of sulphuric acid to obtain a pH=3.

The metallographic microscope observations show the development of red crystals just after 1 day (**Fig.3a**), that grow up to form a uniform layer in B_7d.

Insert here Fig. 3a

From 10 days some green crystals develop above the red layer (**Fig.3b**). The red layer has a variable thickness from 1 μm to 7.6 μm. The green crystals have an increasing thickness up to about 100 μm in B_90d (**Table 1**).

Insert here Fig. 3b

Insert here Table 1

The XRD analysis performed on B_60d allows to clearly identify red crystals as cuprite (Cu_2O) and green crystals as brochantite ($Cu_4SO_4(OH)_6$) due to the corrosion process (XRD patterns are reported in Appendix A, figures S4_2).

The SEM-EDS analyses of samples from B_15d to B_90d confirm the presence of copper sulphate. The analysis on the brocanthite crystals identifies the elements Cu, S and O (**Fig.4b**). The limit of the original surface is preserved (**Fig.4a**).

Insert here Fig. 4

The Cu apparent concentration, obtained with the "Patina" algorithm decreases from 86.6 wt.% (initial measured concentration) to 66.2 wt.% after 90 days of immersion. The Sn/Cu ratio does not change from B_1d to B_90d and the Sn concentration is equal to the initially measured composition in B_90d (12.2 wt.%) using the "Metals" algorithm. In addition, the "Patina" algorithm detects no appreciable change in the Sn concentration (the complete data are reported in table S3_1 in Appendix A). The development of the crystals of cuprite and brochantite (maximum 100 μm in thickness) has no effect on the XRF measurements (**Fig.5**).

Insert here Fig. 5

3.3 Solution C

Macroscopically, a powdery thin green layer covers the specimens at each immersion time. The thickness of this patina varies from 35 μm (C_10d) to 150 μm in C_90d (**Table 2**).

Insert here Table 2

The XRD analysis of the sample C_60d identifies atacamite and paratacamite phases. The presence of atacamite and paratacamite indicates a well-known bronze disease [31-34] which disrupts the surface and can disfigure the artefact [35]. The corrosion layer has a globular structure and the corrosion products have strongly penetrated into the metallic bulk of the alloy.

The SEM-EDS analyses of the samples from C_30d to C_90d detect a corrosion product of Cu and Cl above Sn-Cl corrosion products (**Fig.6a and b**). Probably, the latter develops before 30 days of immersion. This corrosion product is not identified by XRD analysis due to the thickness of the overlying atacamite/paratacamite layer in C_60d.

Insert here Fig. 6

The results of the XRF measurements with the normalised "Patina" algorithm show that the Cu concentration constantly decreases from C_1d (78 wt.%) to C_60d. (67 wt.%). The Sn concentration grows steadily up to C_60d (32 wt.%), then decreases after 80 days (7 wt.%) and it becomes equal to 16 wt.% in C_90d. The Pb concentration ranges from 0.3 wt.% to 0.9 wt.% up to C_60d and after 90 days it becomes equal to 0.05 wt.%. The Cl concentration detected with the "Patina" algorithm increases up to C_10d and is stabilised around 10 wt.%. The XRF measurements performed with the "Metals" algorithm after 90 days detect the Cu and Sn concentrations close to the initial measured composition (Cu=84.5 ± 0.04 wt.%; Sn=15.3 ± 0.05 wt.%).

XRF data obtained with the "Patina" algorithm show the evolution of the corrosion process (the complete data are reported in table S3_2 in Appendix A). In C_1d the selective dissolution of Cu leads to a consequent increasing of the Sn concentration (decuprification) in the surface layer accompanied by the presence of mixed Cu and Sn and Sn oxides identified in other studies as cuprite (Cu_2O) romarchite (SnO), cassiterite (SnO_2) and/or oxyhydroxide as hydroromarchite ($5SnO{\cdot}2H_2O$) [36-38]. Decuprification and the development of Sn species (oxides, chlorides) are in agreement with the Type I patina of ancient bronzes. The SEM micrograph in **Fig.7** shows the same needle morphology of crystals identified by Dunkle on pewter as romarchite (SnO).

Insert here Fig. 7

From C_3d copper chlorides are developed, probably cuprous chloride CuCl (nantokite) in accordance with the increase in the Cl concentration (10 wt.%) [39, 40], that implicates heavy inter-granular corrosion phenomena by chlorine and the embrittlement of the artefact [41]. Subsequently, it develops a layer of atacamite and paratacamite as highlighted by XRD analysis in sample C_60d (XRD patterns are reported in Appendix A, figures S4_3). The same morphology of the corrosion patina is observed after 30 days of immersion. Cuprous chloride develops a pH=3.5–4.0 and from its oxidation and hydrolysis, the copper trihydroxychlorides take place according to the following reaction [31]:

$$4CuCl + O_2 + 4H_2O \leftrightarrow 2Cu_2(OH)_3Cl + H^+ + Cl^-$$

Cross section SEM-EDS analyses on C_60d, and C_90d show an inner layer of Sn chloride species that can be developed previously, between 3 and 15 days of immersion because the Sn concentration continues to increase steadily. The chlorination of Sn(II)/Sn(IV) oxyhydroxide species leads to the formation of Sn chloride oxyhydroxide as abhurite ($Sn_{21}Cl_{16}(OH)_{14}O_6$). Sn chloride oxyhydroxide species were detected on the corrosion patina of the $Cu_{90}Sn_{10}$ alloy exposed in NaCl 0.1 M aqueous solution (pH 6.5) in thermodynamic equilibrium with air at room temperature [42]. Around 90 days, the XRF data become more affected by the corrosion layers and, therefore, the measured alloy composition is less and less consistent with the original alloy composition (**Fig.8**):

Insert here Fig. 8

the Cu concentration increases with the thickness of corrosion layers; at the same time the Sn concentration decreases greatly, probably because the volume analysed by the XRF spectrometer does not cross the inner layer of the Sn chloride species. Consequently, in C_90d, the XRF spectrometer does not detect the Sn concentration of the bulk, but only the Sn-Cl corrosion products (**Fig.9**).

Insert here Fig. 9

3.4 Elemental composition of copper-alloyed Egyptian artefacts

The second part of this study concerns the *in situ* XRF measurements of Egyptian copper-tin alloys with similar composition of corroded bronze samples used in laboratory experiments, as discussed previously.

At the beginning of the last century, the toilet spoon C.6428 was classified by Bénédite as an Egyptian bronze mirror with a concave disk and a slight depression 1 mm thick at the centre [43]. The artefact P.624 is a model of the toilet spoon characterised by the small size.

XRF measurements were made in different points (**Fig.10**) in order to obtain statistical information on the detection of chemical composition of bronze alloys. The results show that the toilet spoons are bronzes containing lead impurities.

Insert here Fig. 10

As the results of the accelerated corrosion of samples C have demonstrated, the green patinas with a high concentration of chlorine (8–11 wt.%) observed in extended areas on the toilet spoon C.6428, could be atacamite and/or paratacamite. The grey patina of the same spoon, by contrast, is characterised by high levels of sulphur (10 wt.%) and the red patina probably is constituted by cuprous oxide (cuprite). The apparent concentration of copper is lower in the point of analysis D (54 wt.%) than other points (62.9–67.3 wt.%). In the toilet spoon C.6428, the tin concentration is lower on the green and dark green patinas, (with values between 4.3 wt.% and 5.4 wt.%) than grey and red patinas (11.3–12.6 wt.%).

The green patina has an extensive presence and a uniform colour on the toilet spoon P.624. The concentration of sulphur is higher in measuring point B (7 wt.%) than other measuring points (4–5 wt.%). Point C shows similar concentrations of chlorine and sulphur. Tin concentration of toilet spoon P.624 is very similar in all measured points (11.2–12.8 wt.% with the normalised "Patina" algorithm; 10.1–11.4 wt.% using the "Metals" algorithm).

In correspondence to the green and dark green patinas of the spoon C.6428, low Sn concentrations were detected with respect to the red and grey patinas. This result can be explained with the decrease in Sn concentration due to the thickness and density of green corrosion patinas that can exceed the penetration depth of the XRF analysis. Indeed, it is well known that the copper chloride species can develop above the cuprite layer and consequently the green patinas have a greater thickness that the other patinas. The grey-green patinas of the spoon P.624 showed similar Sn concentration, suggesting low thickness of the corrosion layers.

As can be seen from **Tables 3 and 4**, the concentrations of the alloying elements measured with both algorithms are comparable and lay within the error bar. It is possible to obtain the average chemical compositions of the two toilet spoons by subtracting the chemical concentrations of soil and patina elements (e.g. Ca, Si, Al, K, P, Cl, S) and after appropriate normalisation of the alloying element concentrations. The average composition of the toilet spoon C.6428 without attenuation effects (points of analysis B and E with the normalised "Patina" algorithm and with the "Metals" algorithm) is Cu=85.1 ± 1.2 wt.%, Sn=14.8 ± 1.2 wt.%, Pb=0.13 ± 0.04 wt.%. The average composition of the toilet spoon P.624 is Cu=87.4 ± 0.9 wt.%, Sn=11.7 ± 1.0 wt.%, Pb=0.8 ± 0.2 wt.%, considering all points of analysis carried out with both algorithms.

Insert here Table 6 and 7

4. Conclusions

The study of the degradation phenomena of $Cu_{88}Sn_{12}$ corroded samples allowed the changing and reliability of the composition analysis detected by X-ray fluorescence spectroscopy to be observed.

XRF measurements on the accelerated corrosion samples made it possible to obtain information about instrumental accuracy in the detection of the chemical composition of metallic bulk. The initial chemical concentrations of the alloying elements up to a thickness of the corrosion patina of about 100 μm were measured on samples exposed to solution B. In solution C, the development of copper chloride and hydroxychloride patinas with high thickness prevented the correct evaluation of the alloying elements.

The combined use of both the "Patina" and "Metals" algorithms made it possible to obtain information about the evolution of corrosion processes (e.g. decuprification and development of Sn corrosion products in samples A and C) and the composition of the patinas.

Furthermore, handheld XRF allowed the *in situ* chemical characterisation of two Egyptian toilet spoon C.6428 and P.624 with an amount of tin between about 12 and 15 wt.%. The most reliable XRF data were measured on red and grey corrosion patinas.

The accuracy of the XRF data is obtained by analysing many points and comparing the chemical composition of different corrosion patinas to achieve statistical information of the alloy bulk.

In conclusion, this work made it possible to establish on which corrosion patinas pXRF can detect concentrations of the alloying elements with greater accuracy.

Acknowledgements

The authors would like to thank the team of the Museo Egizio (Turin), in particular Sara Aicardi, for collaboration in the study of the Egyptian bronze artefacts. We acknowledge the Soprintendenza Archeologia, Belle Arti e Paesaggio per la città metropolitana di Torino, for providing archaeological information of the Egyptian bronzes. The authors are grateful to Elettra Fabbri (Department of Engineering, University of Ferrara) for her collaborations, Gaia Fenoglio (Department of Chemistry, University of Turin), Maurizio Aceto (Dipartimento di Scienze e Innovazione Tecnologica (DISIT), Università degli Studi del Piemonte Orientale) and Giulia Penaglia to the help during the chemical analyses of the Egyptian artefacts.

Appendix A

Supplementary data and supplementary figures or tables to this article can be found online at doi:

Supplementary S1

Calibration of pXRF

A preliminary operation concerned calibration of the portable instrumentation using CRM. Calibration was carried out involving different algorithms and was focused in the evaluation of analytical accuracy.

Tables S1_1 and **S1_2** show the results of the XRF measurements of CRM and for the "Metals" algorithm, the values obtained from the XRF measurements are consistent with the values of the certified concentrations (CC). XRF data detect with the "Patina" algorithm are slightly understated. This problem can be solved normalizing the measured concentration (MC). pXRF calibration using certified standards (CRM) without corrosion patinas allowed to obtain information about precision and accuracy of the methodology.

				Metals-60		**Metals-120**		**Metals-180**	
Code	**Element**	**CC (wt.%)**	**Error (±)**	**MC (wt.%)**	**Error (±)**	**MC (wt.%)**	**Error (±)**	**MC (wt.%)**	**Error (±)**
55XG900J3F	Al*	96.15	-	97.09	0.068	97.04	0.048	95.83	0.075
	Si	0.82	0.034	-	-	-	-	0.8	0.09
	Mn	0.56	0.008	0.52	0.035	0.56	0.025	0.50	0.025
	Cu	0.41	0.07	0.42	0.02	0.42	0.01	0.37	0.01
	Zn	0.39	0.008	0.39	0.01	0.40	0.01	0.38	0.01
	Mg	0.38	0.01	-	-	-	-	0.72	0.85
	Fe	0.29	0.009	0.29	0.02	0.28	0.015	0.26	0.015
	Cr	0.25	0.01	0.43	0.02	0.45	0.01	0.42	0.02
	Ni	0.21	0.005	0.21	0.014	0.21	0.009	0.20	0.009
	Ti	0.16	0.01	0.23	0.01	0.23	0.01	0.17	0.009
	Pb	0.14	0.012	0.14	0.006	0.14	0.004	0.12	0.005
	Sn	0.14	0.014	0.14	0.005	0.14	0.004	0.11	0.005
	Co	0.07	0.001	0.07	0.01	0.07	0.007	0.07	0.006
	Sb	0.029	-	0.031	0.003	0.03	0.002	0.023	0.02
32XALB4G	Cu	77.91	-	77.03	0.88	77.03	0.89	77.01	0.93
	Al	7.96	0.07	-	-	-	-	9.31	0.98
	Ni	7.02	0.09	7.56	0.08	7.57	0.06	6.98	0.09
	Fe	4.68	0.12	4.75	0.05	4.77	0.04	4.65	0.04
	Mn	1.2	0.02	1.3	0.04	1.3	0.03	1.2	0.04
	Si	0.335	0.009	-	-	-	-	0.339	0.09
	Zn	0.305	0.008	0.217	0.042	0.186	0.029	0.192	0.025
	Mg	0.297	0.009	-	-	-	-	-	-
	Pb	0.149	0.008	0.162	0.017	0.139	0.012	0.162	0.021
	Sn	0.093	0.008	0.099	0.013	0.098	0.009	0.102	0.008
	P	0.028	0.002	-	-	-	-	-	-
	Cr	0.0275	0.0012	-	-	-	-	-	-
	As	0.01	0.002	-	-	-	-	-	-
31XB17E	Cu	59.5	0.1	59.4	0.6	59.3	0.6	59.8	0.6

	Zn	34.2	0.1	34.5	0.4	34.6	0.4	34.5	0.4
	Al	6.05	0.04	-	-	-	-	5.69	0.96
	Si	0.007	-	-	-	-	-	-	-
	Pb	0.05	-	0.05	0.01	0.05	0.007	0.04	0.006
	Fe	0.02	-	-	-	0.01	0.005	0.01	0.005
	As	0.015	-	-	-	-	-	-	-
	Sn	0.010	0.002	-	-	-	-	-	-
	Ni	0.01	-	0.02	0.009	0.02	0.007	0.02	0.006
	Mn	<0.001	-	-	-	-	-	-	-
	Bi	<0.001	-	-	-	-	-	-	-
	Sb	<0.001	-	-	-	-	-	-	-
31XB22E	Cu	80.77	0.15	81.01	0.12	80.99	0.083		
	Zn	17.32	0.10	17.61	0.089	17.62	0.062		
	Sn	0.209	0.004	0.226	0.015	0.232	0.011		
	Pb	0.209	0.005	0.269	0.022	0.263	0.015		
	Bi	0.193	0.008	0.266	0.02	0.25	0.014		
	Sb	0.173	0.004	0.178	0.015	0.182	0.011		
	Si	0.171	0.004	-	-	-	-		
	As	0.169	0.004	-	-	-	-		
	Fe	0.168	0.004	0.162	0.012	0.169	0.008		
	Ni	0.166	0.002	0.174	0.014	0.183	0.01		
	P	0.157	0.004	-	-	-	-		
	Al	0.125	0.002	-	-	-	-		
	S	0.104	0.006	-	-	-	-		
	Mn	0.097	0.002	0.096	0.013	0.093	0.009		
	B	0.0033	0.0003	-	-	-	-		
31XMNB4E	Cu	58.95	0.12	59.44	0.16	60.76	0.11		
	Zn	27.12	0.11	28.2	0.13	28.2	0.09		
	Mn	4.14	0.04	4.24	0.063	4.31	0.04		
	Ni	3.23	0.05	3.15	0.04	3.19	0.03		
	Al	2.16	0.03	-	-	-	-		
	Fe	1.73	0.05	1.64	0.04	1.62	0.03		
	Sn	1.080	0.015	1.186	0.026	1.19	0.018		
	Si	0.90	0.02	-	-	-	-		
	Pb	0.640	0.011	0.766	0.033	0.731	0.022		
	Co	0.057	0.002	0.017	0.013	0.022	0.009		
	P	0.0252	0.0011	-	-	-	-		
	Ag	0.0171	0.0011	-	-	-	-		
	As	0.0068	0.0008	-	-	-	-		
	Sb	0.006	-	-	-	0.017	0.008		
33XGM8F	Cu	83.81	0.13	83.56	0.12	83.57	0.08		
	Pb	6.11	0.06	6.44	0.08	6.36	0.06		
	Zn	5.45	0.06	5.39	0.06	5.44	0.041		
	Sn	4.13	0.07	4.24	0.05	4.24	0.03		
	Ni	0.148	0.004	0.149	0.018	0.161	0.012		
	Al	0.0005	0.0002	-	-	-	-		

	Si	0.001	-	-	-	-	-	
	As	0.0159	0.0008	-	-	-	-	
	Mn	0.0008	0.0001	-	-	-	-	
	Bi	0.0248	0.0012	0.029	0.021	0.021	0.014	
	Sb	0.0146	0.0006	0.019	0.012	0.024	0.008	
	P	0.0029	0.0004	-	-	-	-	
	S	0.0119	0.0007	-	-	-	-	
	Cr	0.0004	-	-	-	-	-	
	Ag	0.097	0.003	-	-	-	-	
	Fe	0.098	0.003	0.103	0.012	0.108	0.009	

Tab. S1_1. Chemical compositions of MBH standards with the "Metals" algorithm in different measurement times: 60 seconds (Metals-60; 30s for each energy range), 120 seconds (Metals-120; 60s for each energy range), 180 seconds (Metals-180; 90s for each energy range). Note: CC = Certified Concentration; MC = Measured Concentration.

				Patina-120			Patina-240		
Code	**Element**	**CC (wt.%)**	**Error (±)**	**MC (wt.%)**	**Error (±)**	**Normal. (wt.%)**	**MC (wt.%)**	**Error (±)**	**Normal. (wt.%)**
55XG900J3F	Al*	96.15	-	92.3	0.04	98.05	91.78	0.67	98.13
	Si	0.82	0.034	0.39	0.076	0.41	0.365	0.049	0.39
	Mn	0.56	0.008	0.33	0.02	0.35	0.32	0.016	0.34
	Cu	0.41	0.07	0.22	0.01	0.24	0.22	0.01	0.23
	Zn	0.39	0.008	0.21	0.008	0.22	0.2	0.01	0.21
	Fe	0.29	0.009	0.16	0.01	0.16	0.15	0.01	0.16
	Cr	0.25	0.01	0.14	0.01	0.15	0.14	0.005	0.14
	Ni	0.21	0.005	0.08	0.008	0.08	0.08	0.004	0.08
	Ti	0.16	0.01	0.08	0.008	0.09	0.07	0.004	0.08
	Pb	0.14	0.012	0.07	0.003	0.07	0.07	0.003	0.07
	Sn	0.14	0.014	0.1	0.003	0.11	0.1	0.004	0.1
	Co	0.07	0.001	0.04	0.006	0.05	0.04	0.004	0.04
	Sb	0.029	-	0.02	0.002	0.02	0.02	0.002	0.016
32XALB4G	Cu	77.91	-	73.04	6.54	77.05	73.39	3.35	77.94
	Al	7.96	0.07	10.8	1.62	11.4	9.74	0.98	10.3
	Ni	7.02	0.09	4.41	0.33	4.65	4.41	0.18	4.68
	Fe	4.68	0.12	4.61	0.09	4.86	4.56	0.06	4.84
	Mn	1.2	0.02	1.3	0.04	1.4	1.3	0.03	1.4
	Si	0.335	0.009	0.323	0.123	0.34	0.422	0.081	0.448
	Zn	0.305	0.008	0.07	0.037	0.073	0.057	0.024	0.06
	Mg	0.297	0.009	-	-	-	-	-	-
	Pb	0.149	0.008	0.155	0.027	0.163	0.148	0.016	0.157
	Sn	0.093	0.008	0.121	0.027	0.127	0.125	0.017	0.132
	P	0.028	0.002	-	-	-	-	-	-
	Cr	0.0275	0.0012	-	-	-	-	-	-
	As	0.01	0.002	-	-	-	-	-	-
31XB17E	Cu	59.5	0.1	54.0	3.6	58.8	54.7	2.1	58.9

	Zn	34.2	0.1	31.9	2.4	33.8	31.5	1.2	33.9
	Al	6.05	0.04	6.8	1.6	7.3	6.6	0.9	7.1
	Si	0.007	-	-	-	-	-	-	-
	Pb	0.05	-	0.03	0.01	0.03	0.03	0.006	0.03
	Fe	0.02	-	0.02	0.008	0.02	-	-	-
	As	0.015	-	-	-	-	-	-	-
	Sn	0.010	0.002	-	-	-	0.015	0.01	0.016
	Ni	0.01	-	0.01	0.007	0.01	-	-	-
	Mn	<0.001	-	-	-	-	-	-	-
	Bi	<0.001	-	-	-	-	-	-	-
	Sb	<0.001	-	-	-	-	-	-	-
31XB22E	Cu	80.77	0.15	75.55	6.21	80.52	73.18	2.38	80.63
	Zn	17.32	0.10	16.35	1.39	17.42	15.73	0.53	17.32
	Sn	0.209	0.004	0.289	0.047	0.308	0.292	0.025	0.322
	Pb	0.209	0.005	0.216	0.035	0.23	0.205	0.018	0.225
	Bi	0.193	0.008	0.166	0.027	0.178	0.167	0.014	0.184
	Sb	0.173	0.004	0.224	0.038	0.23	0.21	0.02	0.23
	Si	0.171	0.004	-	-	-	-	-	-
	As	0.169	0.004	0.166	0.032	0.177	0.173	0.018	0.19
	Fe	0.168	0.004	0.165	0.014	0.175	0.156	0.009	0.171
	Ni	0.166	0.002	0.125	0.013	0.172	0.121	0.008	0.168
	P	0.157	0.004	0.216	0.035	0.23	0.205	0.018	0.226
	Al	0.125	0.002	-	-	-	-	-	-
	S	0.104	0.006	0.23	0.042	0.245	0.217	0.027	0.239
	Mn	0.097	0.002	0.103	0.015	0.109	0.089	0.01	0.098
	B	0.0033	0.0003	-	-	-	-	-	-
31XMNB4E	Cu	58.95	0.12	54.96	4.11	58.82	54.82	3.03	58.45
	Zn	27.12	0.11	24.37	1.92	26.08	24.28	1.42	25.88
	Mn	4.14	0.04	4.31	0.11	4.61	4.32	0.08	4.6
	Ni	3.23	0.05	1.98	0.11	2.12	1.98	0.08	2.11
	Al	2.16	0.03	2.92	1.17	3.12	3.6	0.8	3.84
	Fe	1.73	0.05	1.55	0.05	1.66	1.59	0.04	1.69
	Sn	1.080	0.015	1.399	0.169	1.497	1.397	0.122	1.489
	Si	0.90	0.02	1.29	0.18	1.38	1.23	0.12	1.31
	Pb	0.640	0.011	0.582	0.072	0.623	0.563	0.05	0.6
	Co	0.057	0.002	0.02	0.014	0.021	0.011	0.01	0.012
	P	0.0252	0.0011	-	-	-	-	-	-
	Ag	0.0171	0.0011	0.053	0.038	0.0567	0.029	0.021	0.0309
	As	0.0068	0.0008	-	-	-	-	-	-
	Sb	0.006	-	0.014	0.014	0.015	-	-	-
33XGM8F	Cu	83.81	0.13	76.4	5.03	82.83	77.5	6.25	82.79
	Pb	6.11	0.06	5.01	0.43	5.43	5.1	0.53	5.44
	Zn	5.45	0.06	4.94	0.34	5.36	5.02	0.42	5.36
	Sn	4.13	0.07	5.03	0.46	5.45	5.14	0.56	5.49
	Ni	0.148	0.004	0.102	0.014	0.111	0.1	0.011	0.101
	Al	0.0005	0.0002	-	-	-	-	-	-

	Si	0.001	-	-	-	-	-	-	-
	As	0.0159	0.0008	-	-	-	-	-	-
	Mn	0.0008	0.0001	-	-	-	-	-	-
	Bi	0.0248	0.0012	-	-	-	-	-	-
	Sb	0.0146	0.0006	0.024	0.017	0.0260	-	-	-
	P	0.0029	0.0004	-	-	-	-	-	-
	S	0.0119	0.0007	0.547	0.052	0.5931	0.557	0.041	0.5950
	Cr	0.0004	-	-	-	-	-	-	-
	Ag	0.097	0.003	0.107	0.023	0.116	0.103	0.018	0.11
	Fe	0.098	0.003	0.083	0.014	0.09	0.098	0.01	0.105

Tab. S1_2. Chemical compositions of MBH standards with the "Patina" algorithm in different measurement times: 120 seconds (Patina-120; 30s for each energy range) and 240 seconds (Patina-240; 60s for each energy range). Note: CC = Certified Concentration; MC = Measured Concentration; Normal. = Normalized concentration.

Supplementary S2

Determination of the initial measured composition and measurement errors of $Cu_{88}Sn_{12}$ alloy

The nominal composition is Sn = 12 wt.% and the presence of possible impurities such as Pb, Zn, Ni, Sb and Fe lower than 1 wt.%. XRF measurements have defined the following four types of errors:

- algorithm error (E_a): error of the single element assigned by XRF spectrometer after each XRF measurement;
- repeatability error (E_b): error calculated on 5 measurements carried out on the same point of Ød samples[1];
- homogeneity error (E_c): error calculated on measurements carried out on a set of 3 Ød samples;
- roughness error (E_d): error obtained from measurements performed on a set of 5 samples of the $Cu_{88}Sn_{12}$ alloy, with different degree of roughness (not polished, polished with abrasive grinding papers up to 1000 grit and polishing up to 3 μm diamond paste).

The repeatability, homogeneity and roughness errors was calculated using the formula of standard deviation. All measurements were performed with the algorithm "Metals" (60s for measure: 30s for each energy range). After the comparison between the errors obtained it was chosen the worst error to assign with its element of the initial measured composition (E_f) (**Tab.S2_1**). The alloy composition was determined by the arithmetic mean of all the measurements carried out on the alloy samples: Cu = 86.6 ± 0.5 wt.%, Sn = 11.9 ± 0.4 wt.%, Pb = 0.97 ± 0.1 wt%, Ni = 0.2 ± 0.02 wt.%, Zn = 0.19 ± 0.04 wt.%, Sb = 0.09 ± 0.02 wt.%. The Sn concentration is in accord with the NC of the alloy (≈12 wt%). Furthermore, the Pb concentration is close to 1 wt%, while the concentrations of Zn, Ni and Sb are about one or two orders of magnitude lower than lead concentration.

Elements	E_a	E_b	E_c	E_d	E_f
Cu	0.09	0.03	0.5	0.3	0.5
Sn	0.07	0.03	0.4	0.3	0.4
Pb	0.04	0.02	0.1	0.06	0.1
Ni	0.02	0.01	0.01	0.01	0.02
Zn	0.04	0.02	0.04	0.02	0.04
Sb	0.02	0.01	0.01	0.01	0.02

Tab.S2_1. Types of errors of the $Cu_{88}Sn_{12}$ alloy. Note: E_a = algorithm error; E_b = repeatability error; E_c = homogeneity error; E_d = roughness error; E_f = final error.

[1] Ød sample = reference specimen kept intact (without immersion in the corrosive solutions).

Supplementary S3

Quantitative XRF data tables

	Cu (wt.%)	Sn (wt.%)	Pb (wt.%)	Zn (wt.%)	Ni (wt.%)	Sb (wt.%)	Cl (wt.%)	DM (wt.%)
A_1d_p	**76.9** ± 1.2	**14.2** ± 0.2	**0.62** ± 0.02	**0.22** ± 0.03	**0.131** ± 0.01	**0.26** ± 0.01	-	**7.7** ± 1.4
A_1d_pn	**83.5** ± 0.1	**15.4** ± 0.1	**0.68** ± 0.01	**0.24** ± 0.04	**0.14** ± 0.01	**0.10** ± 0.01	-	-
A_1d_m	**86.2** ± 0.1	**12.5** ± 0.1	**0.84** ± 0.03	**0.16** ± 0.01	**0.21** ± 0.01	**0.09** ± 0.01	-	-
A_3d_p	**77.6** ± 0.4	**14.0** ± 0.2	**0.51** ± 0.02	**0.24** ± 0.01	**0.13** ± 0.01	**0.24** ± 0.01	**0.12** ± 0.01	**7.2** ± 0.6
A_3d_pn	**83.9** ± 0.1	**15.1** ± 0.2	**0.55** ± 0.02	**0.26** ± 0.01	**0.14** ± 0.01	**0.09** ± 0.01	-	-
A_3d_m	**86.7** ± 0.1	**12.2** ± 0.1	**0.69** ± 0.01	**0.15** ± 0.01	**0.20** ± 0.01	**0.09** ± 0.01	-	-
A_7d_p	**75.0** ± 2.0	**14.6** ± 0.5	**0.66** ± 0.04	**0.23** ± 0.02	**0.13** ± 0.01	**0.29** ± 0.01	**0.4** ± 0.4	**8.4** ± 2.6
A_7d_pn	**82.7** ± 0.3	**16.1** ± 0.3	**0.73** ± 0.04	**0.25** ± 0.02	**0.14** ± 0.01	**0.10** ± 0.01	-	-
A_7d_m	**85.2** ± 0.1	**13.4** ± 0.1	**0.98** ± 0.02	**0.17** ± 0.01	**0.22** ± 0.02	**0.10** ± 0.01	-	-
A_10d_p	**75.4** ± 1.0	**13.6** ± 0.3	**0.59** ± 0.01	**0.17** ± 0.02	**0.12** ± 0.01	**0.27** ± 0.01	**0.10** ± 0.01	**9.6** ± 1.3
A_10d_pn	**83.8** ± 0.1	**15.1** ± 0.1	**0.65** ± 0.01	**0.19** ± 0.02	**0.14** ± 0.01	**0.10** ± 0.01	-	-
A_10d_m	**86.3** ± 0.1	**12.4** ± 0.1	**0.82** ± 0.02	**0.16** ± 0.01	**0.21** ± 0.01	**0.10** ± 0.01	-	-
A_15d_p	**75.0** ± 1.7	**14.3** ± 0.2	**0.67** ± 0.02	**0.23** ± 0.03	**0.13** ± 0.01	**0.28** ± 0.01	**0.18** ± 0.01	**8.6** ± 2.4
A_15d_pn	**83.0** ± 0.2	**15.8** ± 0.1	**0.74** ± 0.02	**0.26** ± 0.04	**0.14** ± 0.01	**0.10** ± 0.01	-	-
A_15d_m	**85.8** ± 0.3	**12.8** ± 0.2	**0.90** ± 0.04	**0.17** ± 0.03	**0.22** ± 0.01	**0.10** ± 0.02	-	-
A_30d_p	**75.4** ± 0.9	**14.1** ± 0.2	**0.61** ± 0.02	**0.23** ± 0.01	**0.13** ± 0.01	**0.30** ± 0.01	**0.18** ± 0.01	**8.9** ± 1.2
A_30d_pn	**83.3** ± 0.1	**15.5** ± 0.05	**0.67** ± 0.02	**0.26** ± 0.01	**0.15** ± 0.01	**0.11** ± 0.01	-	-
A_30d_m	**86.0** ± 0.1	**12.6** ± 0.02	**0.88** ± 0.03	**0.18** ± 0.01	**0.21** ± 0.01	**0.09** ± 0.01	-	-
A_60d_p	**56.5** ± 0.1	**15.7** ± 0.2	**1.47** ± 0.02	**0.36** ± 0.03	**0.11** ± 0.01	**0.11** ± 0.01	**2.7** ± 0.1	**20.8** ± 0.5
A_60d_pn	**76.1** ± 0.3	**21.2** ± 0.3	**1.98** ± 0.02	**0.48** ± 0.04	**0.14** ± 0.01	**0.15** ± 0.01	-	-
A_60d_m	**77.9** ± 0.1	**18.7** ± 0.1	**2.63** ± 0.03	**0.42** ± 0.01	**0.21** ± 0.01	**0.14** ± 0.01	-	-
A_90d_p	**25.8** ± 0.1	**25.3** ± 0.2	**2.94** ± 0.03	**0.53** ± 0.01	**0.25** ± 0.01	**0.57** ± 0.02	**1.1** ± 0.1	**40.9** ± 0.3
A_90d_pn	**46.9** ± 0.1	**46.0** ± 0.2	**5.34** ± 0.06	**0.96** ± 0.02	**0.45** ± 0.01	**0.35** ± 0.03	-	-
A_90d_m	**47.7** ± 0.1	**43.3** ± 0.2	**6.98** ± 0.06	**0.97** ± 0.02	**0.67** ± 0.05	**0.35** ± 0.01	-	-

Tab.S3_1. XRF measurements of the CuSn12 samples immersed in solution A at different degrees of corrosion. Notes: -p = chemical composition determined using the "Patina" algorithm; -pn = normalized chemical composition determined using the "Patina" algorithm; -m = chemical composition determined using the "Metals" algorithm. DM = Dark Matrix concentration.

	Cu (wt.%)	Sn (wt.%)	Pb (wt.%)	Zn (wt.%)	Ni (wt.%)	Sb (wt.%)	Cl (wt.%)	S (wt.%)	DM (wt.%)
B_1d_p	**74.3** ± 1.4	**13.0** ± 0.4	**0.65** ± 0.01	**0.20** ± 0.01	**0.12** ± 0.01	**0.09** ± 0.02	0.1 ± 0.03	1.09 ± 0.02	9.9 ± 1.9
B_1d_pn	**84.1** ± 0.2	**14.8** ± 0.2	**0.73** ± 0.004	**0.22** ± 0.01	**0.14** ± 0.01	**0.10** ± 0.02	-	-	-
B_1d_m	**86.4** ± 0.1	**12.2** ± 0.1	**0.96** ± 0.02	**0.16** ± 0.03	**0.20** ± 0.01	**0.09** ± 0.01	-	-	-
B_3d_p	**75.2** ± 0.6	**15.2** ± 0.2	**0.71** ± 0.02	**0.20** ± 0.01	**0.12** ± 0.01	**0.08** ± 0.01	0.20 ± 0.01	1.04 ± 0.03	6.8 ± 0.8
B_3d_pn	**82.2** ± 0.1	**16.6** ± 0.1	**0.77** ± 0.011	**0.21** ± 0.01	**0.13** ± 0.01	**0.09** ± 0.01	-	-	-
B_3d_m	**85.1** ± 0.1	**13.5** ± 0.02	**1.00** ± 0.01	**0.15** ± 0.01	**0.21** ± 0.01	**0.10** ± 0.01	-	-	-
B_7d_p	**75.0** ± 1.4	**13.8** ± 0.4	**0.59** ± 0.01	**0.18** ± 0.02	**0.12** ± 0.01	**0.10** ± 0.01	0.10 ± 0.01	0.73 ± 0.02	9.2 ± 1.9
B_7d_pn	**83.5** ± 0.1	**15.3** ± 0.10	**0.66** ± 0.01	**0.20** ± 0.02	**0.14** ± 0.01	**0.11** ± 0.02	-	-	-
B_7d_m	**86.1** ± 0.1	**12.6** ± 0.1	**0.82** ± 0.02	**0.14** ± 0.01	**0.20** ± 0.01	**0.09** ± 0.01	-	-	-
B_10d_p	**74.0** ± 0.2	**14.0** ± 0.2	**0.73** ± 0.01	**0.15** ± 0.02	**0.11** ± 0.01	**0.09** ± 0.01	0.16 ± 0.01	1.63 ± 0.01	8.8 ± 0.4
B_10d_pn	**83.1** ± 0.2	**15.7** ± 0.14	**0.82** ± 0.01	**0.17** ± 0.02	**0.12** ± 0.01	**0.10** ± 0.01	-	-	-
B_10d_m	**85.7** ± 0.1	**12.9** ± 0.1	**1.03** ± 0.02	**0.14** ± 0.02	**0.20** ± 0.01	**0.09** ± 0.01	-	-	-
B_15d_p	**72.9** ± 0.7	**13.8** ± 0.1	**0.68** ± 0.01	**0.19** ± 0.01	**0.11** ± 0.01	**0.09** ± 0.02	0.03 ± 0.01	3.54 ± 0.07	8.3 ± 0.9
B_15d_pn	**83.0** ± 0.1	**15.8** ± 0.1	**0.77** ± 0.01	**0.21** ± 0.02	**0.12** ± 0.01	**0.10** ± 0.02	-	-	-
B_15d_m	**85.5** ± 0.1	**13.1** ± 0.1	**0.98** ± 0.02	**0.15** ± 0.01	**0.19** ± 0.02	**0.09** ± 0.002	-	-	-
B_30d_p	**73.7** ± 0.5	**13.0** ± 0.2	**0.55** ± 0.01	**0.18** ± 0.02	**0.11** ± 0.01	**0.09** ± 0.02	0.13 ± 0.01	2.88 ± 0.02	9.1 ± 0.6
B_30d_pn	**84.1** ± 0.1	**14.8** ± 0.2	**0.63** ± 0.01	**0.21** ± 0.02	**0.13** ± 0.01	**0.10** ± 0.03	-	-	-
B_30d_m	**86.4** ± 0.1	**12.3** ± 0.04	**0.84** ± 0.02	**0.13** ± 0.02	**0.18** ± 0.01	**0.09** ± 0.01	-	-	-
B_60d_p	**70.4** ± 1.7	**12.2** ± 0.5	**0.49** ± 0.01	**0.19** ± 0.02	**0.08** ± 0.01	**0.07** ± 0.01	0.35 ± 0.01	4.37 ± 0.03	11.8 ± 2.3
B_60d_pn	**84.4** ± 0.2	**14.6** ± 0.2	**0.59** ± 0.01	**0.22** ± 0.02	**0.09** ± 0.01	**0.09** ± 0.02	-	-	-
B_60d_m	**86.6** ± 0.1	**12.3** ± 0.1	**0.77** ± 0.01	**0.12** ± 0.01	**0.15** ± 0.01	**0.08** ± 0.01	-	-	-

B_90d_p	**66.2** ± 0.6	**10.8** ± 0.1	**0.48** ± 0.01	**0.07** ± 0.01	**0.05** ± 0.01	**0.07** ± 0.01	-	5.8 ± 0.1	16.5 ± 0.7
B_90d_pn	**85.2** ± 0.1	**13.9** ± 0.1	**0.61** ± 0.015	**0.09** ± 0.01	**0.07** ± 0.01	**0.09** ± 0.02	-	-	-
B_90d_m	**86.8** ± 0.1	**12.2** ± 0.1	**0.81** ± 0.004	**-**	**0.09** ± 0.01	**0.09** ± 0.01	-	-	-

Tab.S3_2. XRF measurements of the CuSn12 samples immersed in solution B at different degrees of corrosion. Notes: -p = chemical composition determined using the "Patina" algorithm; -pn = normalized chemical composition determined using the "Patina" algorithm; -m = chemical composition determined using the "Metals" algorithm. DM = Dark Matrix concentration.

	Cu (wt.%)	Sn (wt.%)	Pb (wt.%)	Zn (wt.%)	Ni (wt.%)	Sb (wt.%)	Cl (wt.%)	DM (wt.%)
C_1d_p	**53.6** ± 1.5	**14.3** ± 0.5	**0.33** ± 0.01	**0.19** ± 0.01	**0.06** ± 0.01	**0.10** ± 0.01	**0.2** ± 0.1	**22.3** ± 1.7
C_1d_pn	**78.2** ± 0.2	**20.9** ± 0.2	**0.48** ± 0.004	**0.28** ± 0.01	**0.09** ± 0.01	**0.15** ± 0.02	-	-
C_1d_m	**79.5** ± 0.1	**19.4** ± 0.1	**0.64** ± 0.01	**0.22** ± 0.03	**0.11** ± 0.01	**0.14** ± 0.01	-	-
C_3d_p	**53.0** ± 0.3	**16.3** ± 0.2	**0.42** ± 0.01	**0.21** ± 0.01	**0.08** ± 0.005	**0.1** ± 0.01	**9.8** ± 0.1	**19.7** ± 0.6
C_3d_pn	**75.6** ± 0.2	**23.3** ± 0.2	**0.60** ± 0.01	**0.30** ± 0.02	**0.11** ± 0.01	**0.15** ± 0.01	-	-
C_3d_m	**77.1** ± 0.1	**21.5** ± 0.1	**0.84** ± 0.02	**0.25** ± 0.01	**0.16** ± 0.01	**0.17** ± 0.01	-	-
C_7d_p	**57.4** ± 0.6	**15.6** ± 0.2	**0.58** ± 0.01	**0.25** ± 0.01	**0.10** ± 0.01	**0.11** ± 0.01	**13.3** ± 0.1	**12.3** ± 0.6
C_7d_pn	**77.5** ± 0.1	**21.1** ± 0.1	**0.78** ± 0.02	**0.34** ± 0.01	**0.14** ± 0.01	**0.15** ± 0.02	-	-
C_7d_m	**78.8** ± 0.1	**19.5** ± 0.1	**1.05** ± 0.04	**0.31** ± 0.02	**0.21** ± 0.01	**0.13** ± 0.01	-	-
C_10d_p	**47.4** ± 0.4	**15.7** ± 0.2	**0.48** ± 0.03	**0.26** ± 0.01	**0.14** ± 0.01	**0.09** ± 0.01	**14.4** ± 0.1	**21.3** ± 0.6
C_10d_pn	**73.9** ± 0.1	**24.5** ± 0.1	**0.75** ± 0.04	**0.41** ± 0.01	**0.23** ± 0.02	**0.14** ± 0.02	-	-
C_10d_m	**74.5** ± 0.1	**23.7**± 0.1	**1.02** ± 0.02	**0.38** ± 0.01	**0.33** ± 0.02	**0.15** ± 0.01	-	-
C_15d_p	**42.6** ± 1.3	**19.1** ± 0.3	**0.92** ± 0.04	**0.28** ± 0.01	**0.10** ± 0.01	**0.13** ± 0.02	**9.7** ± 0.1	**26.9** ± 1.7
C_15d_pn	**67.5** ± 0.3	**30.2** ± 0.3	**1.45** ± 0.03	**0.45** ± 0.03	**0.16** ± 0.009	**0.21** ± 0.02	-	-
C_15d_m	**68.5** ± 0.5	**28.7** ± 0.6	**1.98** ± 0.06	**0.40** ± 0.01	**0.24** ± 0.001	**0.20** ± 0.01	-	-
C_30d_p	**43.7** ± 0.9	**18.5** ± 0.5	**0.77** ± 0.03	**0.26** ± 0.02	**0.15** ± 0.01	**0.11** ± 0.02	**12.1** ± 0.1	**24.1** ± 1.5
C_30d_pn	**68.8** ± 0.2	**29.1** ± 0.2	**1.20** ± 0.02	**0.42** ± 0.03	**0.24** ± 0.01	**0.18** ± 0.03	-	-
C_30d_m	**69.7** ± 0.1	**27.7** ± 0.1	**1.63** ± 0.01	**0.39** ± 0.01	**0.34** ± 0.02	**0.20** ± 0.01	-	-
C_60d_p	**41.1** ± 0.8	**19.5** ± 0.6	**0.40** ± 0.01	**0.04** ± 0.01	-	**0.14** ± 0.01	**11.4** ± 0.1	**27.2** ± 1.5
C_60d_pn	**67.2** ± 0.3	**31.9** ± 0.3	**0.65** ± 0.01	**0.06** ± 0.01	-	**0.22** ± 0.02	-	-
C_60d_m	**68.0** ± 0.1	**30.9** ± 0.1	**0.91** ± 0.01	-	-	**0.20** ± 0.01	-	-
C_90d_p	**56.4** ± 0.6	**10.8** ±0.2	**0.05** ± 0.005	-	-	**0.07** ± 0.01	**8.7** ± 0.1	**23.9** ± 0.05
C_90d_pn	**83.7** ± 0.1	**16.1** ± 0.1	**0.07** ± 0.01	-	-	**0.10** ± 0.02	-	-
C_90d_m	**84.5** ± 0.1	**15.3** ± 0.1	**0.10** ± 0.01	-	-	**0.11** ± 0.01	-	-

Tab.S3_3. XRF measurements of the CuSn12 samples immersed in solution C at different degrees of corrosion. Notes: -p = chemical composition determined using the "Patina" algorithm; -pn = normalized chemical composition determined using the "Patina" algorithm; -m = chemical composition determined using the "Metals" algorithm. DM = Dark Matrix concentration.

Supplementary S4

XRD patterns

Insert here FIG S4_1

Fig. S4_1. Diffraction pattern of sample A_60d exposed to solution A. Not evidence of patinas are visible.

Insert here FIG S4_2

Fig. S4_2. Diffraction pattern of sample B_60d exposed to solution B.

Insert here FIG S4_3

Fig. S4_3. Diffraction pattern of sample C_60d exposed to solution C.

Bibliography

[1] G. Vittiglio, K. Janssens, B. Vekemans, F. Adams, A. Oost, A compact small-beam XRF instrument for in-situ analysis of objects of historical and/or artistic value, Spectrochimica Acta Part B 54 (1999) 1697-1710.

[2] S. Shalev, S.S. Shilstein, Y. Yekutieli, XRF study of archaeological and metallurgical material from an ancient copper-smelting site near Ein-Yahav, Israel, Talanta 70 (2006) 909-913.

[3] T. Čechák, M. Hložek, L. Musílek, T. Trojek, X-ray fluorescence in investigations of archaeological finds, Nuclear Instruments and Methods in Physics Research B 263 (2007) 54-57.

[4] A. Vasilescu, B. Constantinescu, XRF-based compositional microanalysis for provenance studies of metallic artifacts, Romanian Reports in Physics 63 (4) (2011) 901-911.

[5] S. Ridolfi, Portable X-ray Fluorescence Spectrometry for the analyses of Cultural Heritage, IOP Conf. Series: Materials Science and Engineering 37 (2012) 012001, International Conference on the Use of X-ray (and related) Techniques in Arts and Cultural Heritage (XTACH 11).

[6] M. Ferretti, The investigation of ancient metal artefacts by portable X-ray fluorescence devices, J. Anal. At. Spectrom. 29 (2014) 1753-1766.

[7] D. Šatović, V. Desnica, S. Fazinić, Use of portable X-ray fluorescence instrument for bulk alloy analysis on low corroded indoor bronzes, Spectrochimica Acta Part B 89 (2013) 7–13.

[8] R. Fernandes, B.J.H van Os, H.DJ Huisman, The use of Hand-Held XRF for investigating the composition and corrosion of Roman copper-alloyed artefacts, Heritage Science 1 (1) (2013).

[9] E. Angelini, A. Batmaz, A. Çilingiroğlu S. Grassini, G. M. Ingo, C. Riccucci, Tailored analytical strategies for the investigation of metallic artefacts from the Ayanis Fortress in Turkey, Surface and Interface Analysis 42 (6-7) (2010) 675-679.

[10] M.F. Alberghina, R. Barraco, M. Brai, T. Schillaci, L. Tranchina, Integrated analytical methodologies for the study of corrosion processes in archaeological bronzes, Spectrochimica Acta Part B 66 (2011) 129–137.

[11] F. Faraldi, A. Çilingiroğlu, E. Angelini, C. Riccucci, T. De Caro, A. Batmaz, A. Mezzi, D. Caschera, B. Cortese, Micro-chemical and micro-structural investigation of archaeological bronze weapons from the Ayanis fortress (lake Van, Eastern Anatolia, Turkey), Applied Physics A 113 (2013) 911-921.

[12] L. Robbiola, J.M. Blengino, C. Fiaud, Morphology and mechanisms of formation of natural patinas on archaeological Cu-Sn alloys, Corrosion Science 40 (12) (1998) 2083-2111.

[13] C. Soffritti, E. Fabbri, M. Merlin, G.L. Garagnani, C. Monticelli, On the degradation factors of an archaeological bronze bowlbelonging to a private collection, Applied Surface Science 313 (2014) 762-770.

[14] G. Brunton, G. Caton-Thompson, The Badarian civilisation and predynastic remains near Badari, British School of Archaeology in Egypt, London, 1928.

[15] H.C.H. Carpenter, An Egyptian axe head of great antiquity, Nature 130 (1932) 625-626.

[16] A. Lucas, J.R. Harris, Ancient Egyptian materials and industries, fourth ed., Arnord, London, 1962.

[17] J. Riederer, Die naturwissenschaftliche Untersuchung der Bronzen des Ägyptischen Museums Preußischer Kulturbesitz in Berlin, Berliner Beiträge zur Archäometrie 3 (1978) 5-42.

[18] J. Riederer, Metal analysis of Egyptian bronzes, Revue d'Archaeometrie 3 (1981) 239-243.

[19] J. Riederer, Die naturwissenschaftliche Untersuchung der Staatlichen Sammlung Ägyptischer Kunst in München, Berliner Beitriige zur Archäometrie 7 (1982) 5-34.

[20] J. Riederer, Metallanalysen ägyptischen Statuetten des Kestner-Museums, Berliner Beiträge zur Archäometrie 8 (1983) 5-17.

[21] J. Riederer, Die naturwissenschaftliche Untersuchung der Ägyptischen Bronzen des Pelizaeus-Museums in Hildesheim, Berliner Beiträge zur Archäometrie 9 (1984) 5-16.

[22] J. Riederer, Metallanalysen ägyptischen Bronzestatuetten aus Deutschen Museen, Berliner Beiträge zur Archäometrie 10 (1988) 5-20.

[23] E.R. Eaton, H. McKerrell, Near Eastern Alloying and Some Textual Evidence for the Early Use of Arsenical Copper, World Archaeology 8 (2) (1976) 169-191.

[24] R.M. Cowell, Scientific appendix I: chemical analyses, in: W.V. Davies, Catalogue of Egyptian Antiquities in the British Museum. VII, Tools and Weapons. I, Axes, British Museum Publications, London, 1987, pp. 96-118.

[25] J. Ogden, Metals, in: P.T. Nicholson, I. Shaw (Eds.), Ancient Egyptian Materials and Technology, Cambridge University Press, Cambridge, 2000, pp. 148-176.

[26] S.J. Fleming, J. Crowfoot-Payne, PIXE analyses of some Egyptian bronzes of the Late Period, MASCA Journal 1 (2) (1979) 46-47.

[27] V. Hayez, V. Costa, J. Guillaume, H. Terryn, A. Hubin, Micro Raman spectroscopy used for the study of corrosion products on copper alloys: study of the chemical composition of artificial patinas used for restoration purposes, Analyst 130 (2005) 550-556.

[28] K. Leyssens, A. Adriaens, C. Degrigny, E. Pantos, Evaluation of Corrosion Potential Measurements as a Means to Monitor the Storage and Stabilization Processes of Archaeological

Copper-Based Artifacts, Analytical Chemistry 78 (8) (2006) 2794-2801.

[29] M. Ghoniem, The characterization of a corroded Egyptian bronze statue and a study of the degradation phenomena, International Journal of Conservation Science 2 (2) 95-108.

[30] V. K. Gouda, G. I. Youssef, N. A. Abdel Ghany, Characterization of Egyptian bronze archaeological artifacts, Surface and Interface analysis 44 (2012) 1338-1345.

[31] D.A. Scott, Bronze disease: a review of some chemical problems and the role of relative humidity, Journal of the American Institute for Conservation 29 (1990) 193-206.

[32] D.A. Scott, A review of copper chlorides and related salts in bronze corrosion and as painting pigments, Studies in Conservation 45 (1) (2000) 39-53.

[33] A. Mezzi, E. Angelini, C. Riccucci, S. Grassini, T. De Caro, F. Faraldi, P. Bernardini, Micro structural and micro-chemical composition of bronze artefacts from Tharros (Western Sardinia, Italy), Surface and Interface Analysis 44 (2012) 958-962.

[34] R. Grayburn, M. Dowsett, M. Hand, P.J. Sabbe, P.Thompson, A. Adriaens, Tracking the progression of bronze disease – A synchrotron X-ray diffraction study of nantokite hydrolysis, Corrosion Science 91 (2015) 220-223.

[35] M.P. Casaletto, T. De Caro, G.M. Ingo, C. Riccucci, Production of reference “ancient” Cu-based alloys and their accelerated degradation methods, Applied Physics A 83 (2006) 617-622.

[36] S.E. Dunkle, J.R. Craig, J.D. Rimstidt, W.R. Lusardi, Romarchite, hydroromarchite and abhurite formed during the corrosion of pewter artifacts from the Queen Anne’s revenge (1718), The Canadian Mineralogist 41 (2003) 659-669.

[37] S.E. Dunkle, J.R. Craig, W.R. Lusardi, Romarchite and associated phases as common corrosion products on pewter artifacts from marine archaeological sites, Geoarchaeology: An International Journal 19 (6) (2004) 531-552.

[38] C. Riccucci, G.M. Ingo, A. Faustoferri, M.I. Pierigè, E.I. Parisi, G. Di Carlo, T. De Caro, F. Faraldi, Micro-chemical and metallurgical study of Samnite bronze belts from ancient Abruzzo (central Italy, VIII–IV BC), Applied Physics A 113 (2013) 959-970.

[39] J. Wang, C. Xu, G. Lv, Formation processes of CuCl and regenerated Cu crystals on bronze surfaces in neutral and acidic media, Applied Surface Science 252 (2006) 6294-6303.

[40] X. Zhang, I. O. Wallinder, C. Leygraf, Mechanistic studies of corrosion product flaking on copper and copper-based alloys in marine environments, Corrosion Science 85 (2014) 15-25.

[41] G.M. Ingo, A. Çilingiroğlu, F. Faraldi, C. Riccucci, M.P. Casaletto, A. Erdem, A. Batmaz, The bronze shields found at the Ayanis fortress (Van region, Turkey): manufacturing techniques and corrosion phenomena, Applied Physics A 100 (2010) 793-800.

[42] L. Robbiola, T.T.M. Tran, P. Dubot, O. Majerus, K. Rahmouni, Characterisation of anodic layers on Cu–10Sn bronze (RDE) in aerated NaCl solution, Corrosion Science 50 (2008) 2205-2215.

[43] M.G. Bénédite, Catalogue Générale des Antiquités Égyptiennes du Musée du Caire. N^{os} 44001-44102. Miroirs, Imprimerie de l'Institut Français d'Archéologie Orientale, 1907.

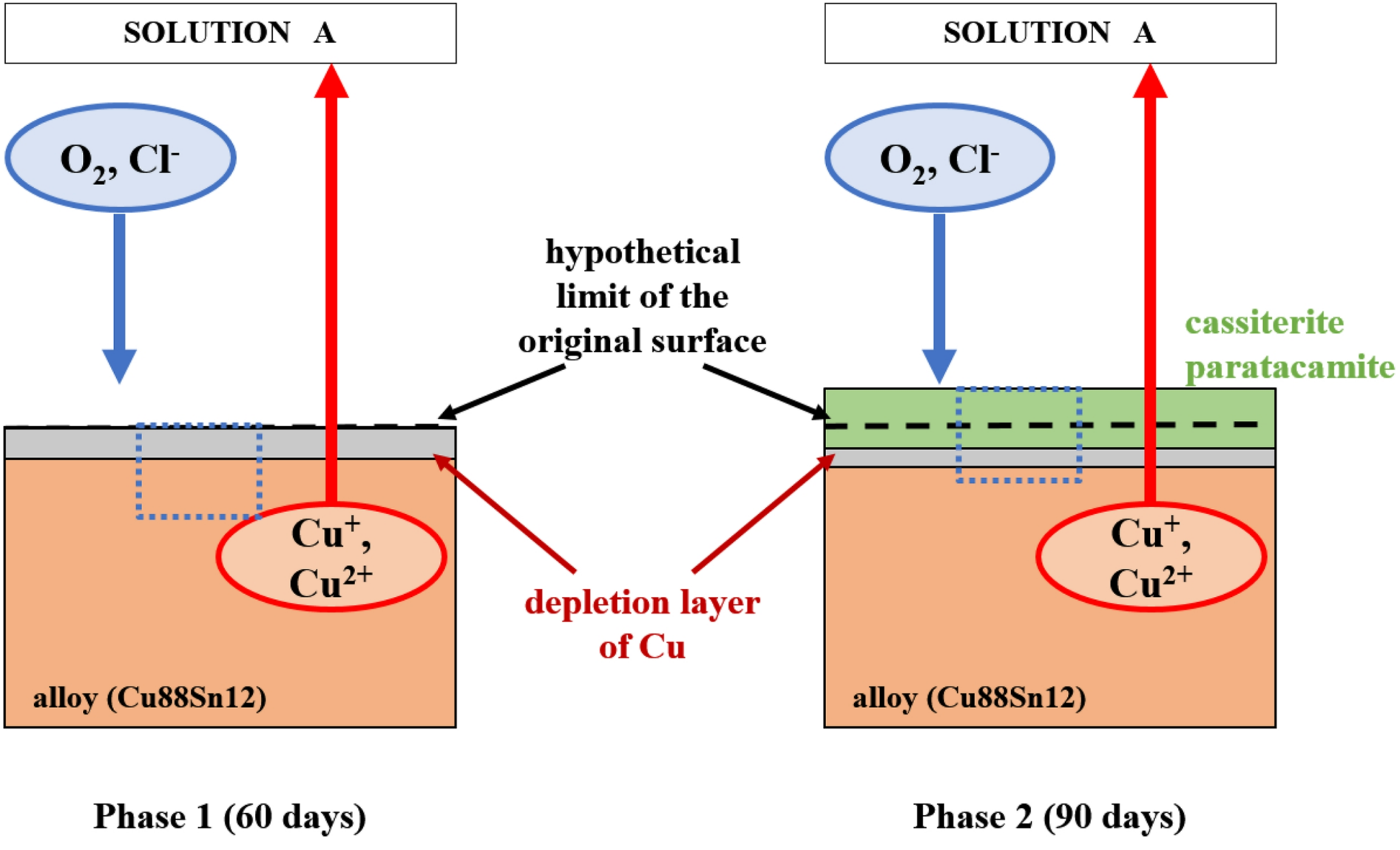
SOLUTION A
SOLUTION A
O2, Cl-
O2, Cl-
hypothetical
limit of the
original surface
cassiterite
paratacamite
Cu+,
Cu2+
Cu+,
Cu2+
depletion layer
of Cu
alloy (Cu88Sn12)
alloy (Cu88Sn12)
Phase 1 (60 days)
Phase 2 (90 days)

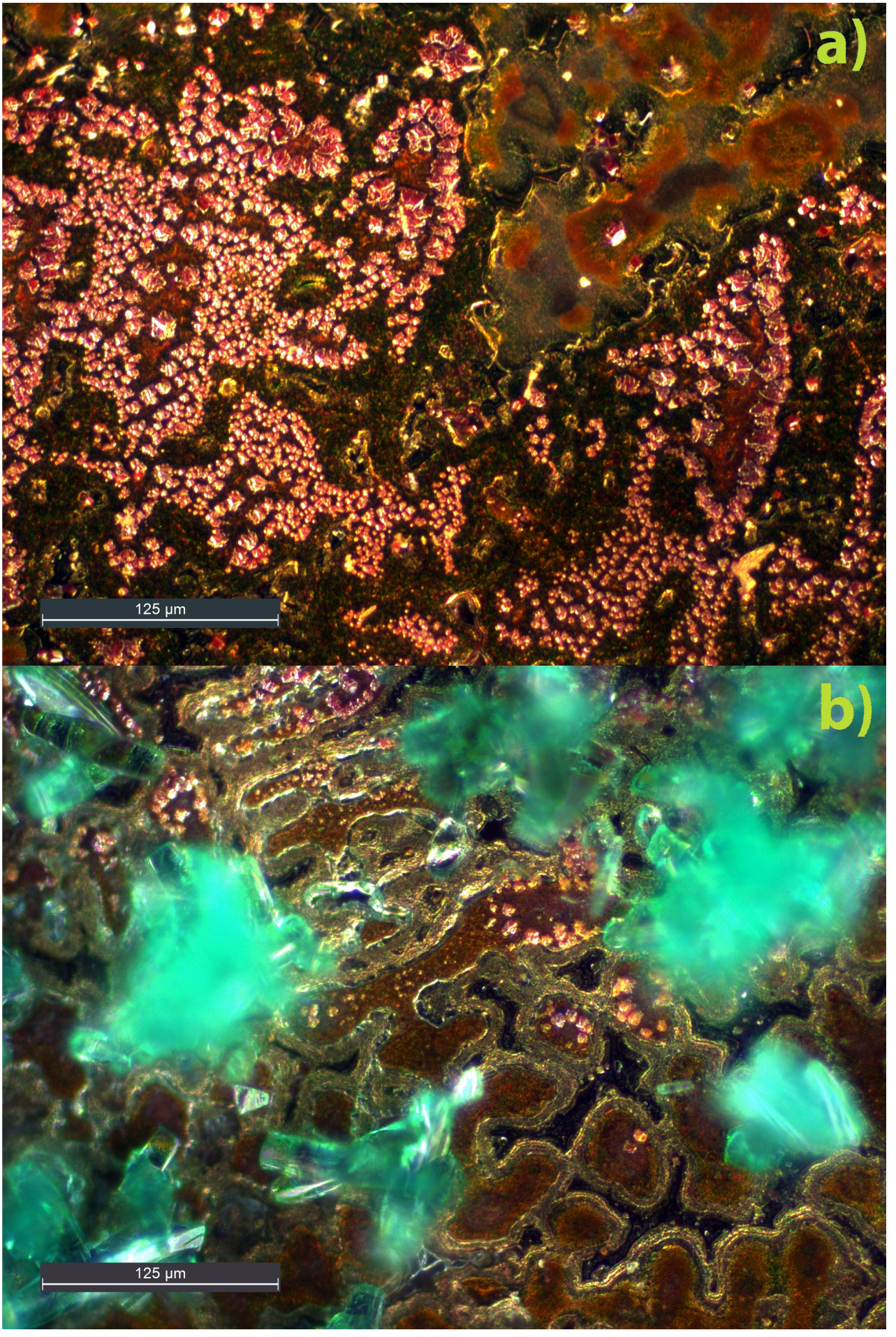
a)
125 µm
b)
125 µm

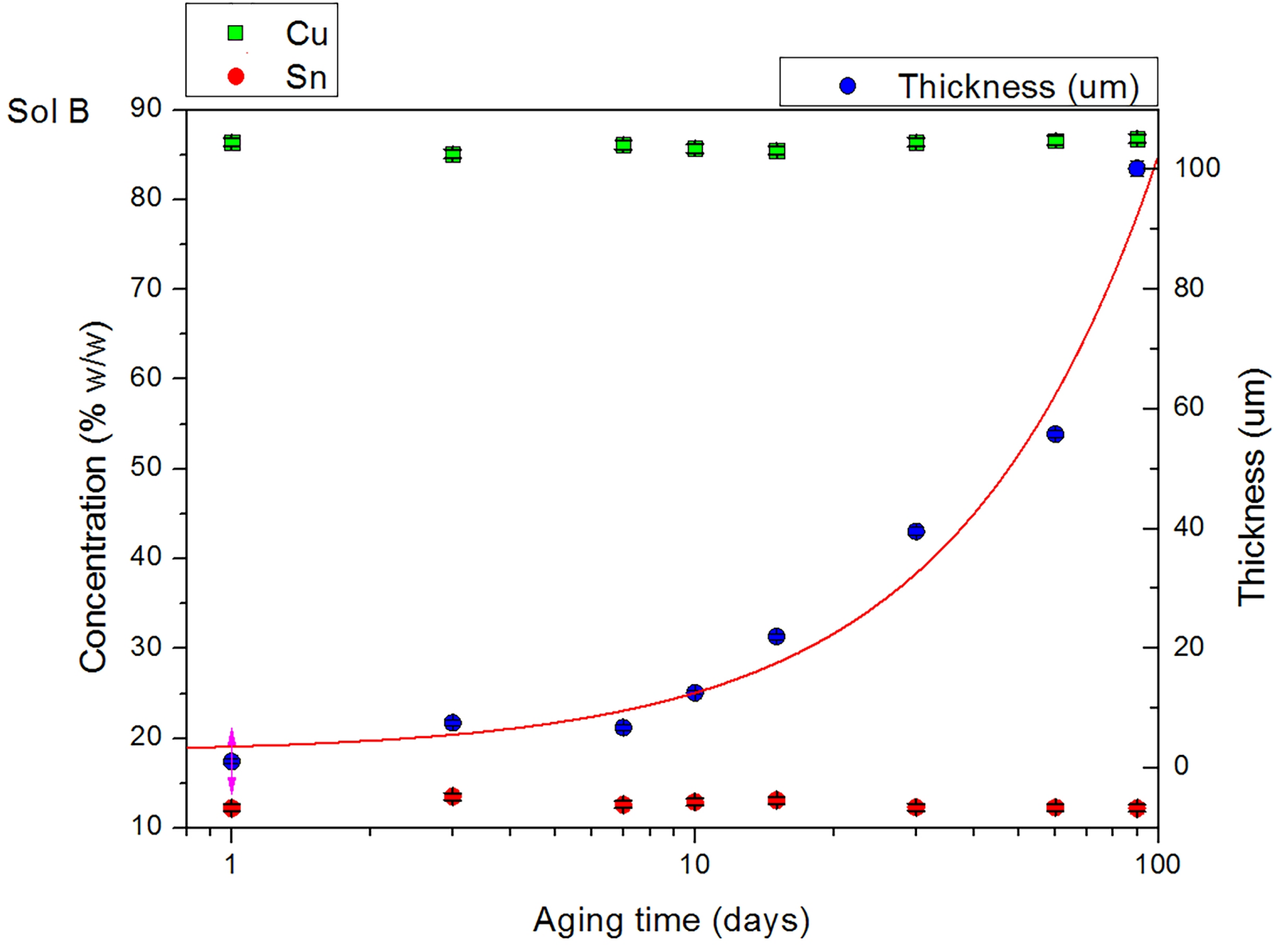
Sol B
Cu
Sn
Thickness (um)
Concentration (% w/w)
Thickness (um)
Aging time (days)
90
80
70
60
50
40
30
20
10
100
80
60
40
20
0
1
10
100

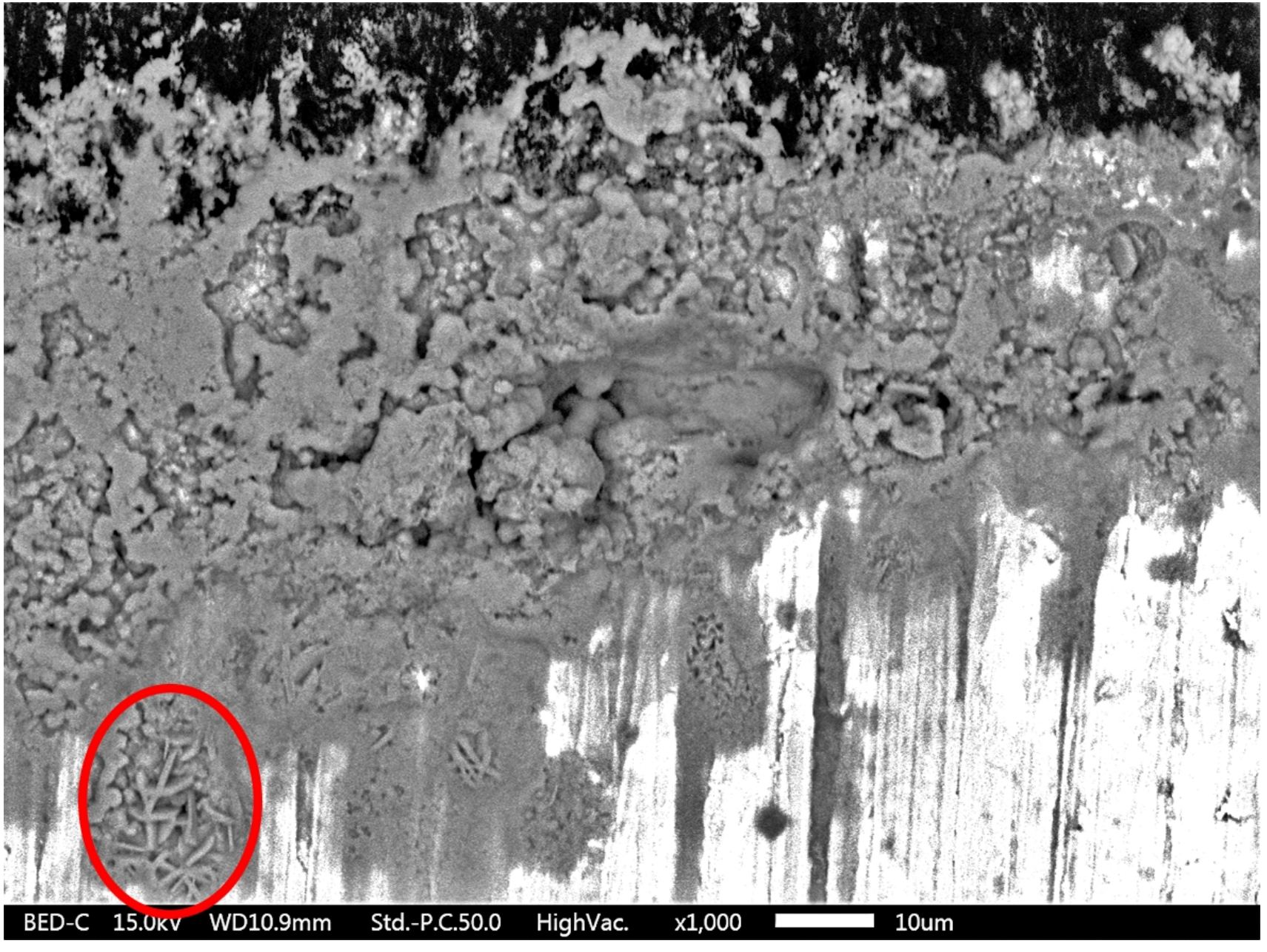
BED-C 15.0kv WD10.9mm Std.-P.C.50.0 HighVac. x1,000 10um

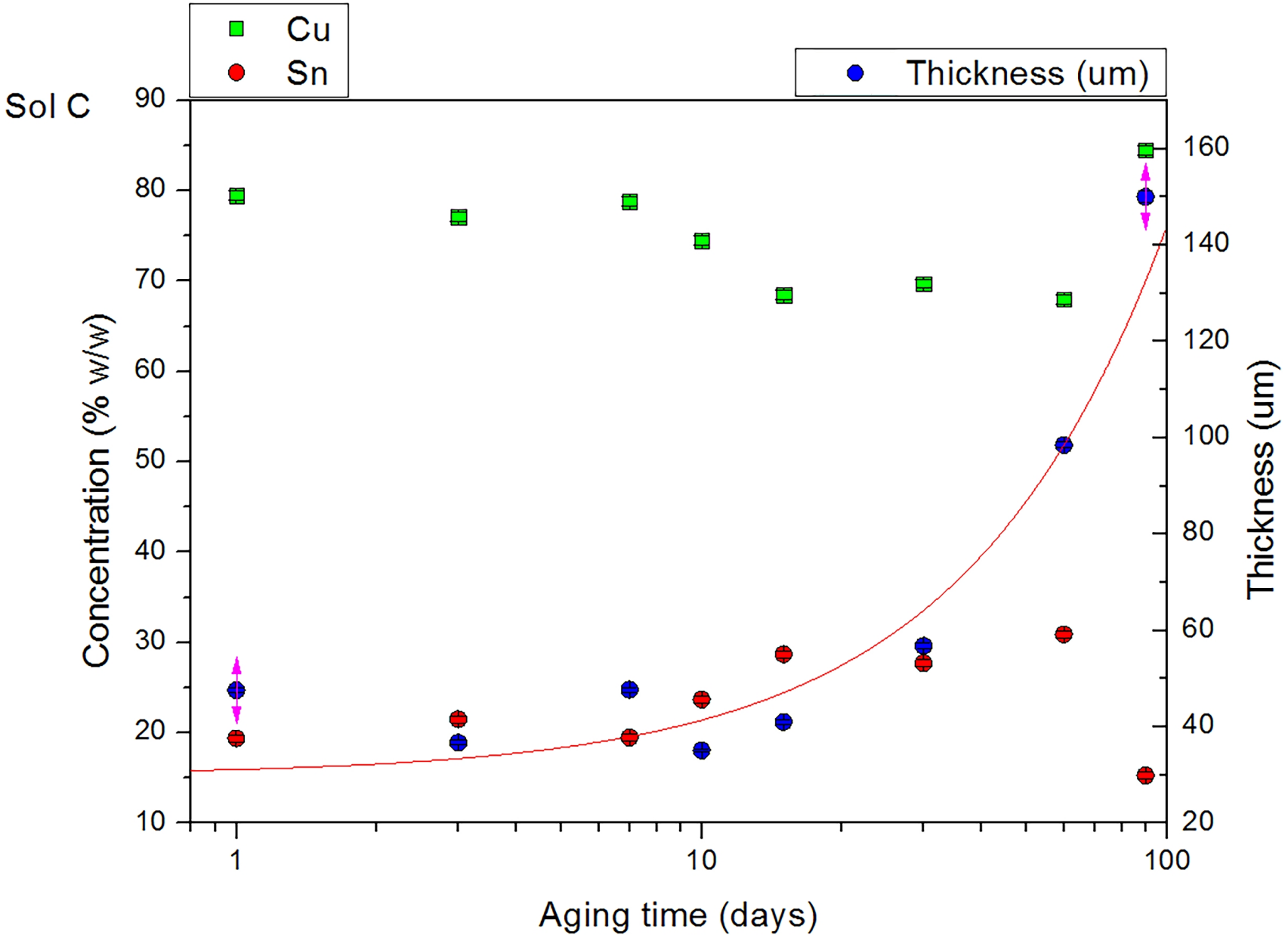
Sol C
Cu
Sn
Thickness (um)
Concentration (% w/w)
Thickness (um)
Aging time (days)
90
80
70
60
50
40
30
20
10
160
140
120
100
80
60
40
20
1
10
100

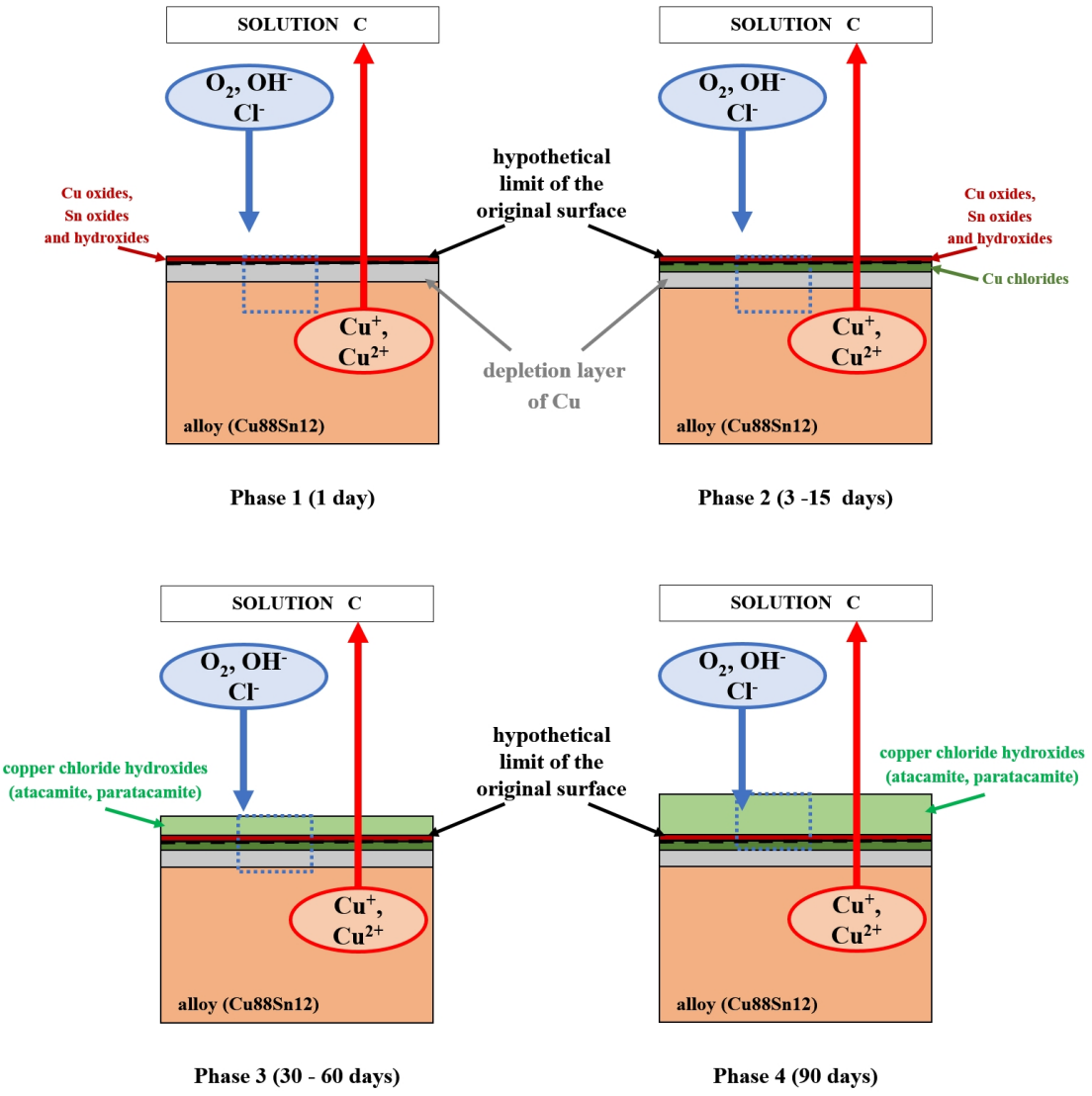
SOLUTION C
O_2, OH^-
Cl^-
Cu oxides,
Sn oxides
and hydroxides
hypothetical
limit of the
original surface
depletion layer
of Cu
Cu^+,
Cu^{2+}
alloy (Cu88Sn12)
Phase 1 (1 day)
SOLUTION C
O_2, OH^-
Cl^-
Cu oxides,
Sn oxides
and hydroxides
Cu chlorides
Cu^+,
Cu^{2+}
alloy (Cu88Sn12)
Phase 2 (3 -15 days)
SOLUTION C
O_2, OH^-
Cl^-
copper chloride hydroxides
(atacamite, paratacamite)
hypothetical
limit of the
original surface
Cu^+,
Cu^{2+}
alloy (Cu88Sn12)
Phase 3 (30 - 60 days)
SOLUTION C
O_2, OH^-
Cl^-
copper chloride hydroxides
(atacamite, paratacamite)
Cu^+,
Cu^{2+}
alloy (Cu88Sn12)
Phase 4 (90 days)

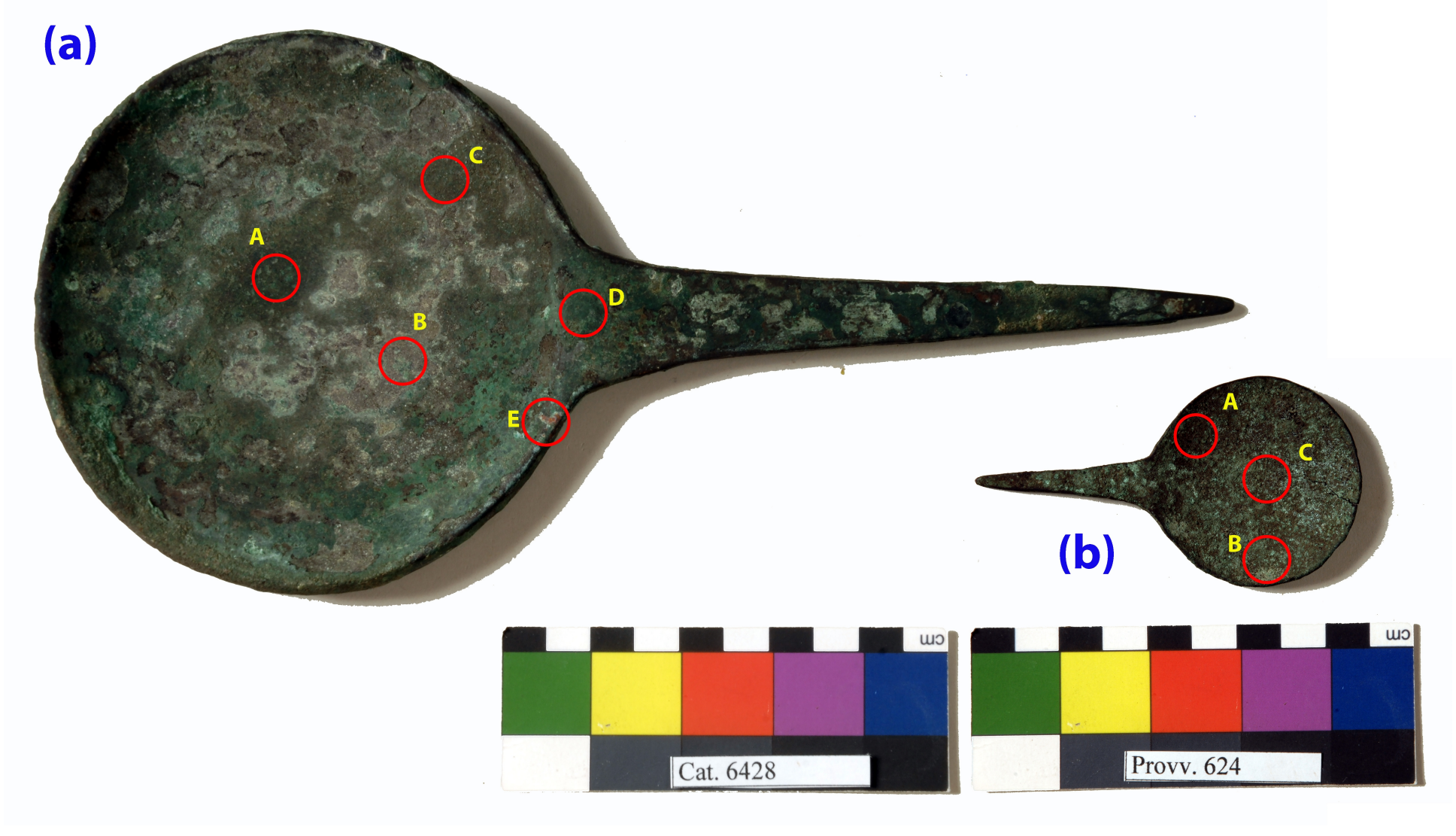
(a)
A
B
C
D
E
(b)
A
B
C
cm
Cat. 6428
cm
Provv. 624

Figures Captions

Fig.1. SEM micrograph (**a**) and EDS line mapping (**b**) of the sample A_90d with the indication of patinas evolution.

Fig.2. Schematic representation of the corrosion layers developed in the solution A during 90 days of immersion. The blue rectangle is the volume analysed by pXRF spectrometer.

Fig.3. Metallographic microscope micrographs of the bronze surface covered by cuprate crystals after 1 day (**a**), and brochantite green crystals developed above the red layer after 10 days (**b**).

Fig.4. SEM micrograph (**a**) and EDS diagram (**b**) of B_90d with the indication of patinas evolution.

Fig.5. Cu and Sn concentration vs aging time in solution B correlated with the increasing of corrosion layer thickness. The red curve indicates the linear regression of the patina growth.

Fig.6. SEM micrograph (**a**) and EDS diagram (**b**) of the sample C_90d with the indication of patinas evolution.

Fig.7. Cross-section micrograph of the corrosion layers of the sample C_30d. Red circled area probably shows needles of romarchite (SnO).

Fig.8. Cu and Sn concentration vs aging time in solution C correlated with the increasing of corrosion layer thickness. The red curve indicates the linear regression of the patina growth.

Fig.9. Schematic representation of the corrosion layers developed in solution C during 90 days of immersion. The blue rectangle is the volume analysed by pXRF spectrometer.

Fig.10. Frontside of the two Egyptian toilet spoons C.6428 (**a**) and P.624 (**b**) with points of analysis.

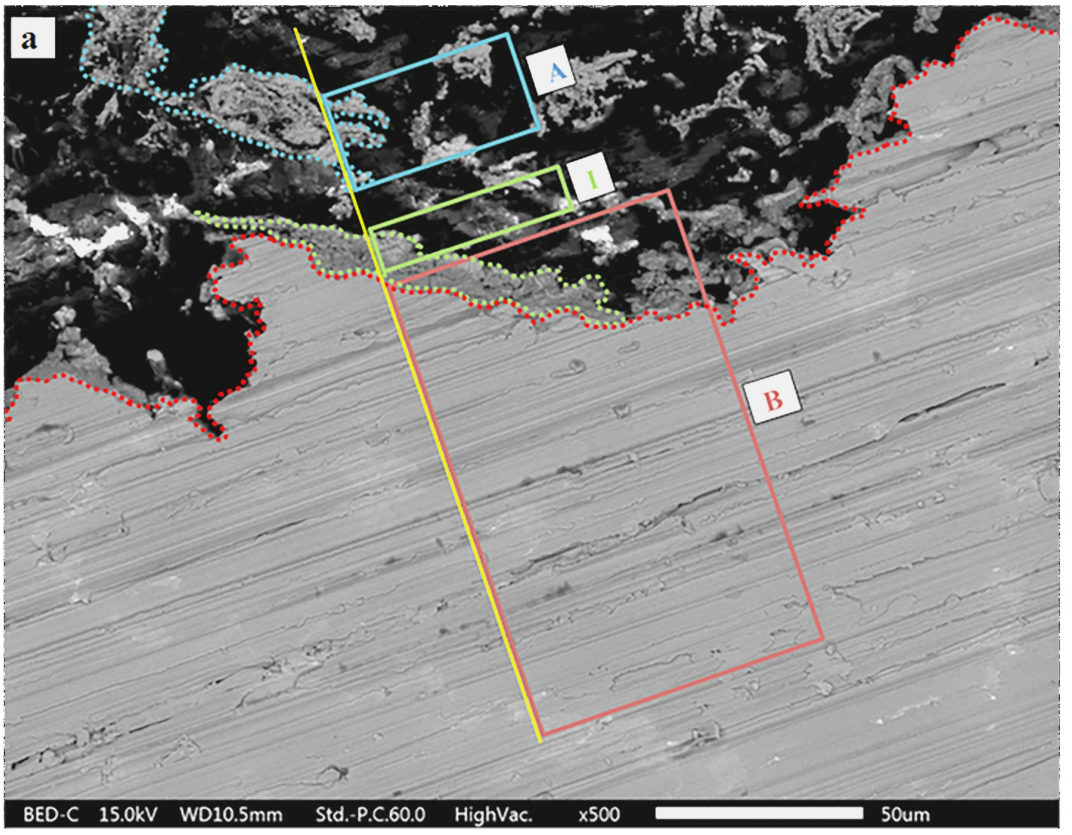
a
A
I
B
BED-C 15.0kV WD10.5mm Std.-P.C.60.0 HighVac. x500 50um

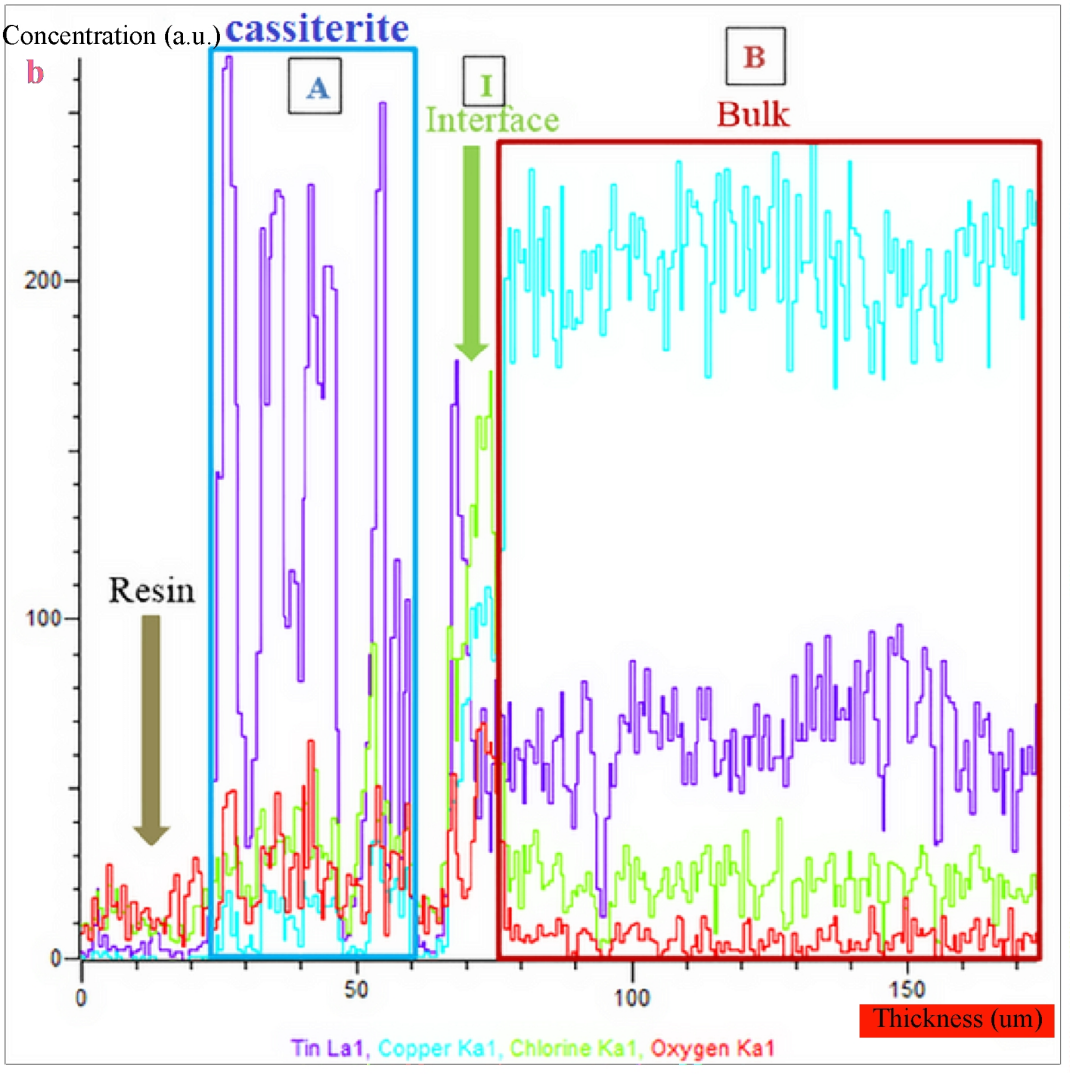
Concentration (a.u.)
b
cassiterite
A
I
Interface
B
Bulk
Resin
200
100
0
0
50
100
150
Thickness (um)
Tin La1, Copper Ka1, Chlorine Ka1, Oxygen Ka1

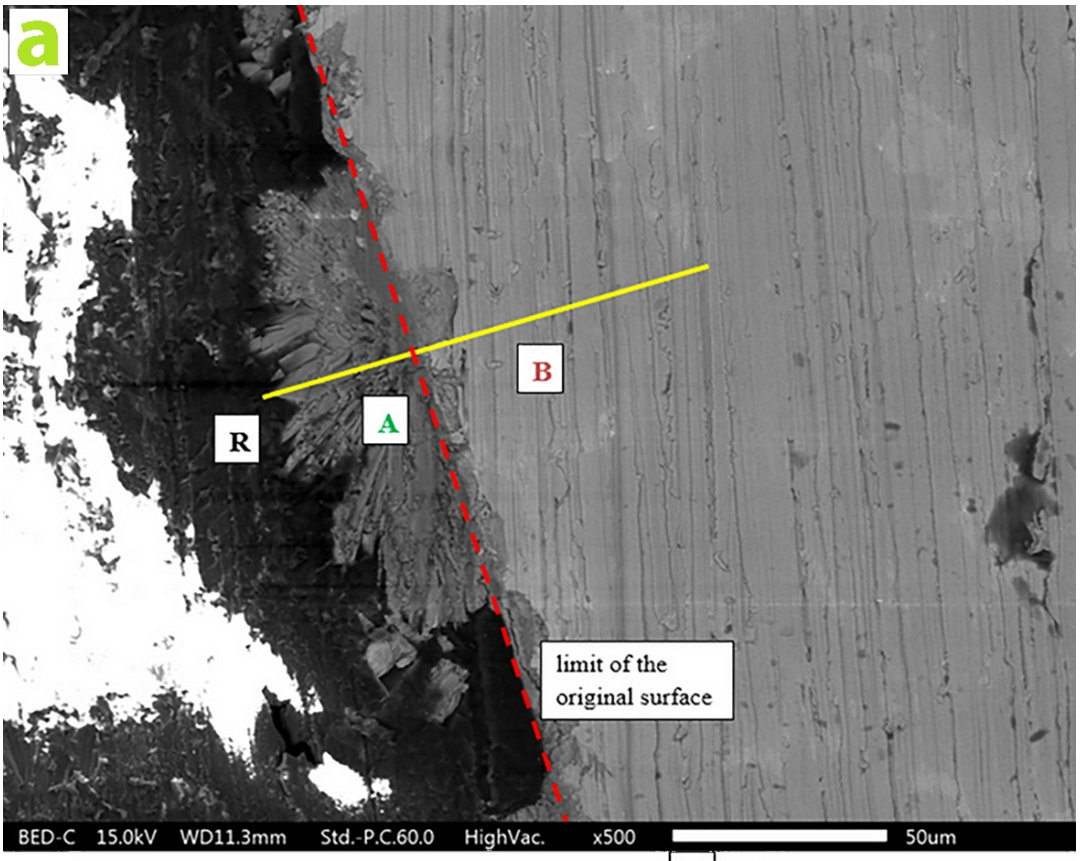
a
R
A
B
limit of the
original surface
BED-C 15.0kV WD11.3mm Std.-P.C.60.0 HighVac. x500 50um

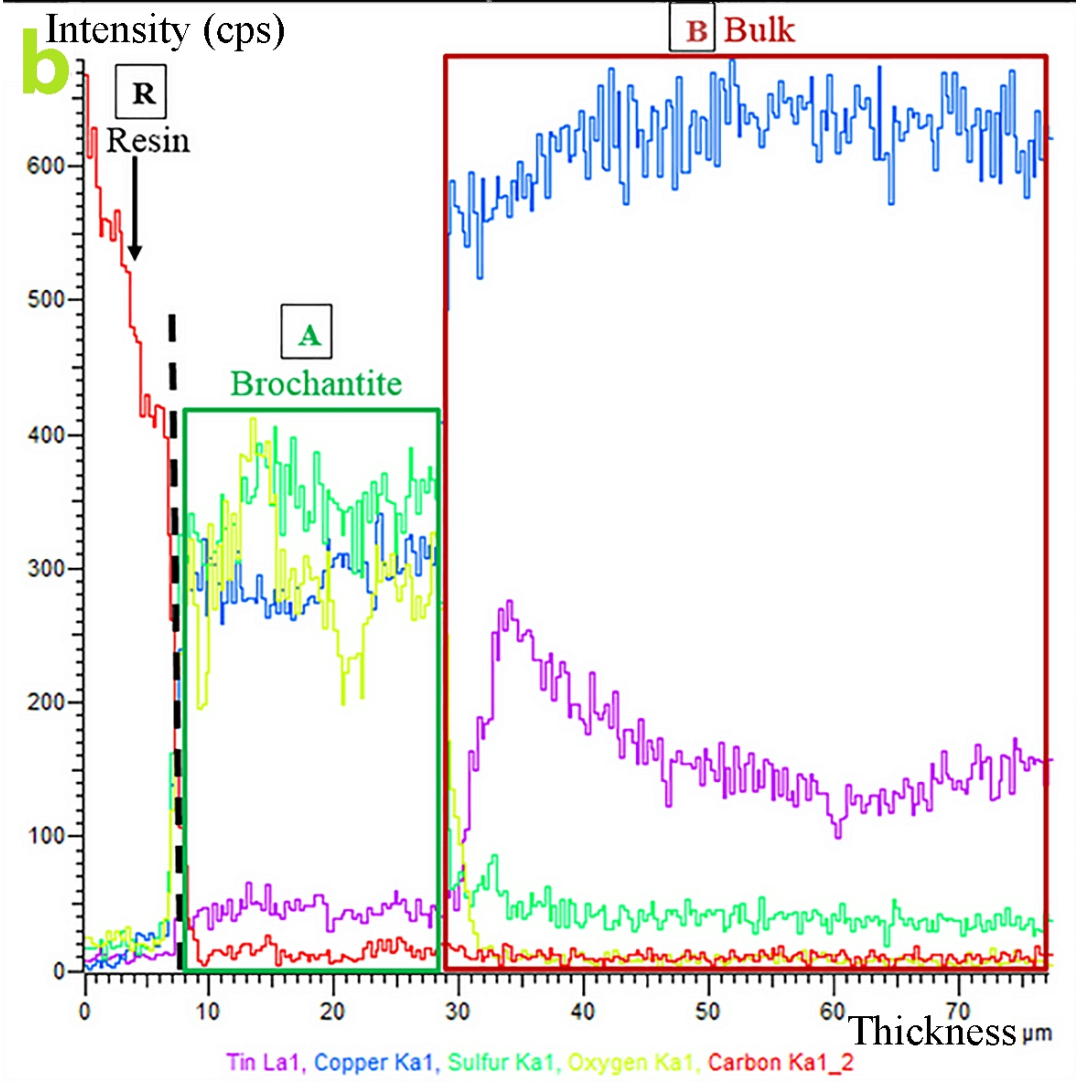
b
Intensity (cps)
R
Resin
A
Brochantite
B Bulk
600
500
400
300
200
100
0
0
10
20
30
40
50
60
70
Thickness µm
Tin La1, Copper Ka1, Sulfur Ka1, Oxygen Ka1, Carbon Ka1_2

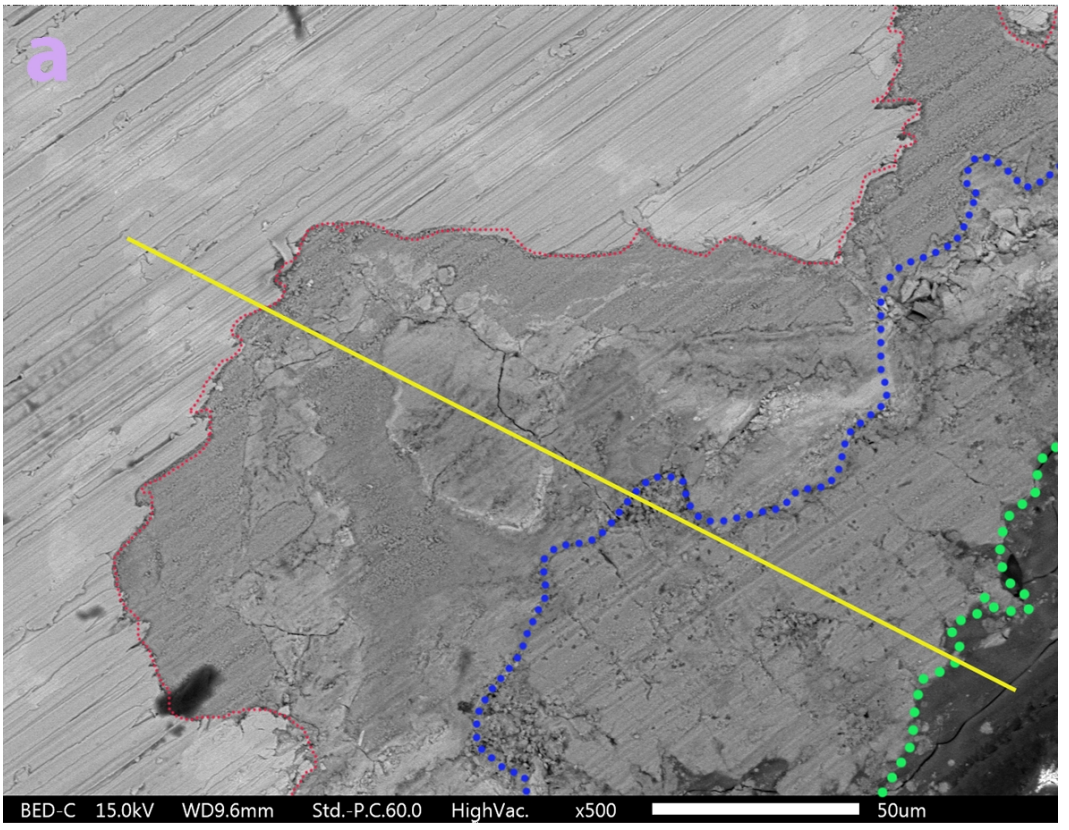
a
BED-C 15.0kV WD9.6mm Std.-P.C.60.0 HighVac. x500 50um

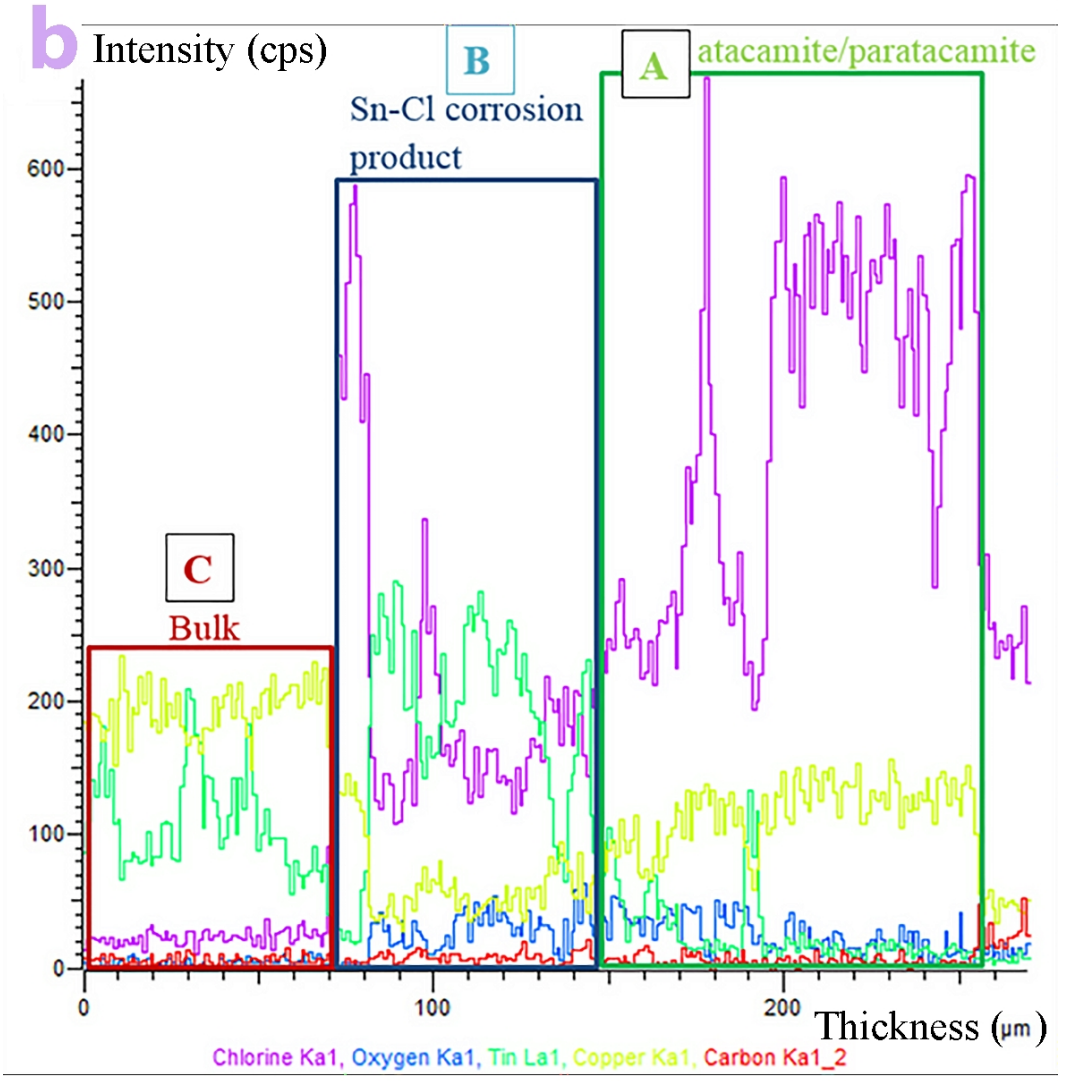
b
Intensity (cps)
B
Sn-Cl corrosion product
A
atacamite/paratacamite
C
Bulk
600
500
400
300
200
100
0
0
100
200
Thickness (µm)
Chlorine Ka1, Oxygen Ka1, Tin La1, Copper Ka1, Carbon Ka1_2

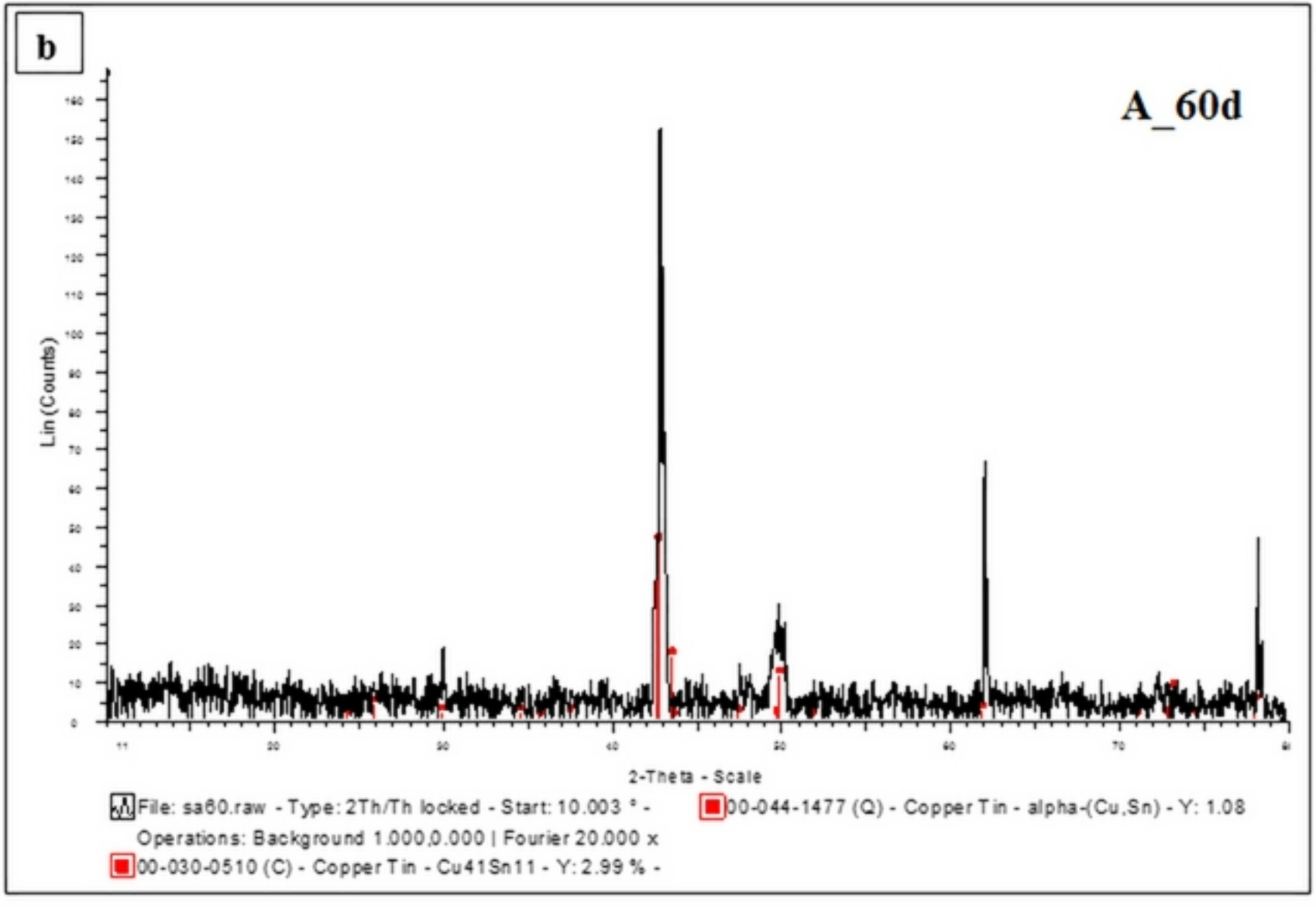
b
A_60d
Lin (Counts)
2-Theta - Scale
File: sa60.raw - Type: 2Th/Th locked - Start: 10.003 ° -
Operations: Background 1.000,0.000 | Fourier 20.000 x
00-030-0510 (C) - Copper Tin - Cu41Sn11 - Y: 2.99 % -
00-044-1477 (Q) - Copper Tin - alpha-(Cu,Sn) - Y: 1.08

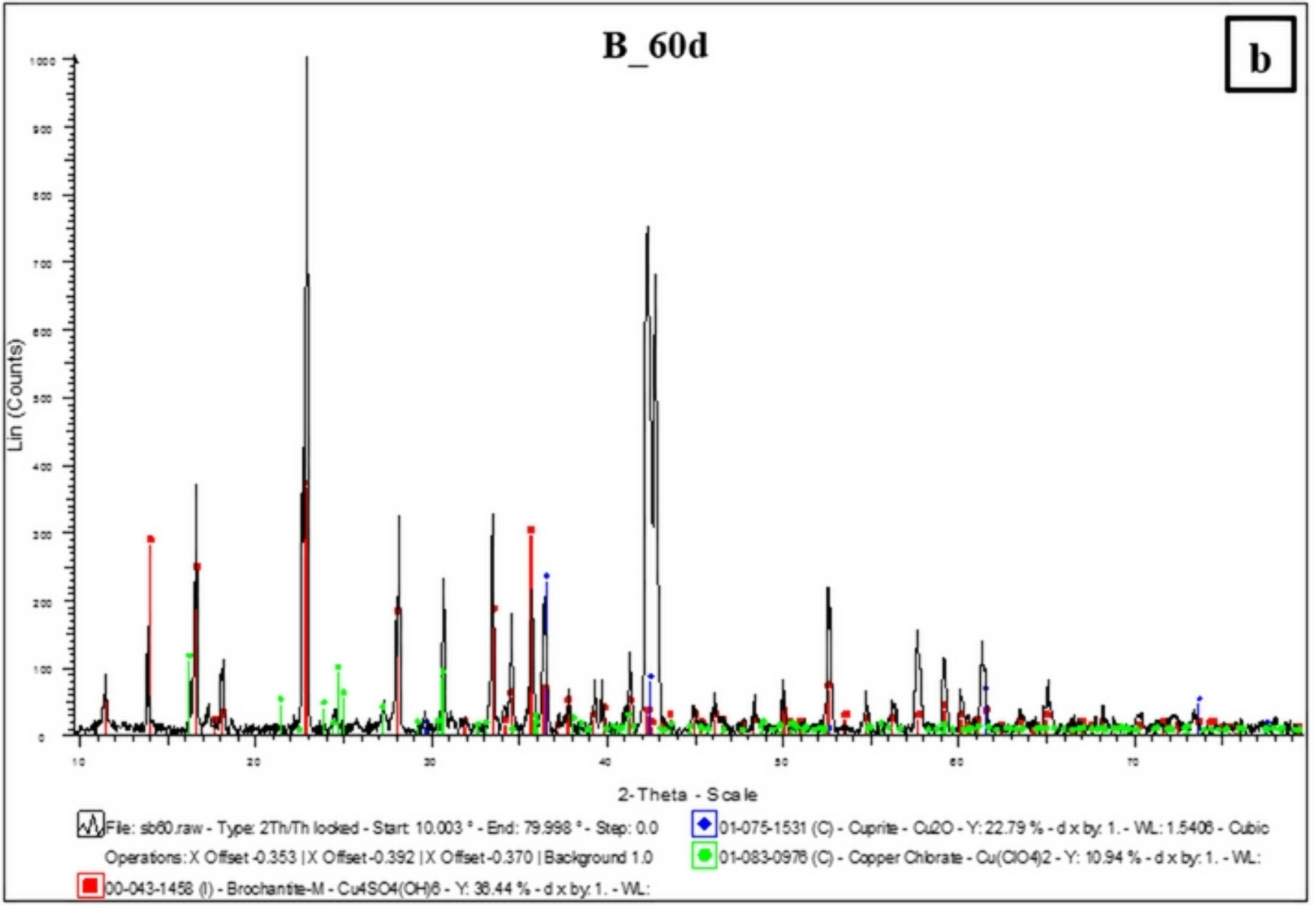
B_60d
b
Lin (Counts)
2-Theta - Scale
File: sb60.raw - Type: 2Th/Th locked - Start: 10.003 ° - End: 79.998 ° - Step: 0.0
Operations: X Offset -0.353 | X Offset -0.392 | X Offset -0.370 | Background 1.0
00-043-1458 (I) - Brochantite-M - Cu4SO4(OH)6 - Y: 36.44 % - d x by: 1. - WL:
01-075-1531 (C) - Cuprite - Cu2O - Y: 22.79 % - d x by: 1. - WL: 1.5406 - Cubic
01-083-0976 (C) - Copper Chlorate - Cu(ClO4)2 - Y: 10.94 % - d x by: 1. - WL:

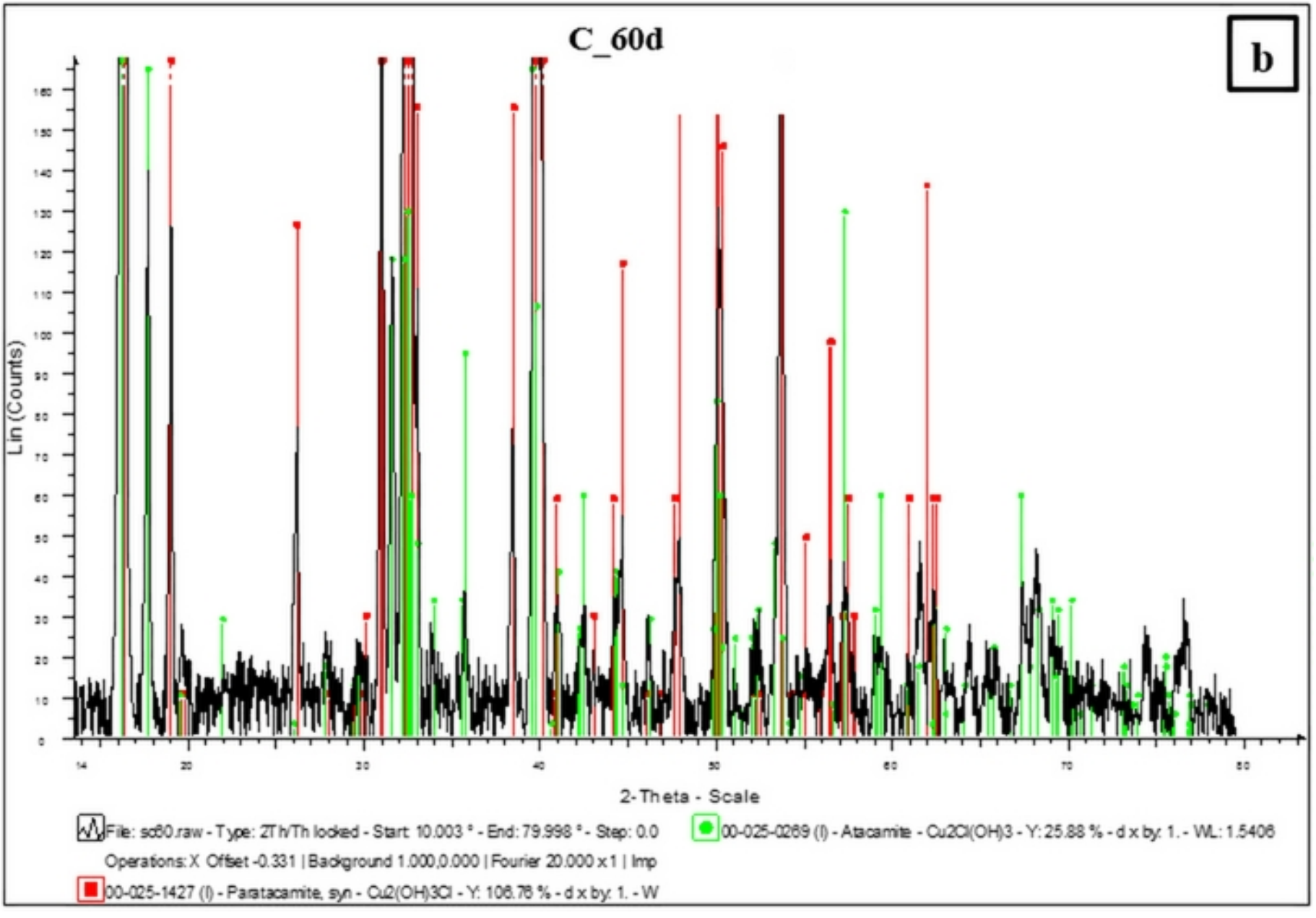
C_60d
b
Lin (Counts)
2-Theta - Scale
File: sc60.raw - Type: 2Th/Th locked - Start: 10.003 ° - End: 79.998 ° - Step: 0.0
Operations: X Offset -0.331 | Background 1.000,0.000 | Fourier 20.000 x 1 | Imp
00-025-1427 (I) - Paratacamite, syn - Cu2(OH)3Cl - Y: 106.76 % - d x by: 1. - W
00-025-0269 (I) - Atacamite - Cu2Cl(OH)3 - Y: 25.88 % - d x by: 1. - WL: 1.5406

Tables

Degree of corrosion	1	2	3	4	5	6	7	8	9
Red layer (µm)	1.1	7.6	6.8	6.2	2.9	2.7	6.4	4.6	2.1
Green crystals layer (µm)	-	-	-	6.4	19.1	36.9	49.4	81.8	98.1

Tab.1. Average thickness of the corrosion products of the CuSn12 samples immersed in solution B, measured in cross-section using the metallograhic microscope.

Degree of corrosion	1	2	3	4	5	6	7	8	9
Green layer (µm)	47.6	36.7	47.7	35.1	41	56.8	98.5	115	150

Tab.2. Average thickness of the corrosion products of the CuSn12 samples immersed in solution C, measured in cross-section using the metallograhic microscope.

Artefact ID	Measuring point	Patina	Cu	$Cu_{(N)}$	Sn	$Sn_{(N)}$	Pb	$Pb_{(N)}$	Fe	Cl	S	Ca	Si	K
C.6428	A	green	**67.3**	**93.6**	**4.6**	**6.3**	**0.02**	**0.03**	0.07	7.8	2.6	0.7	1.1	0.1
	B	grey	**64.7**	**85.1**	**11.3**	**14.8**	**0.06**	**0.08**	0.27	1.1	10.0	1.2	0.9	0.3
	C	green	**62.9**	**91.9**	**5.4**	**8.0**	**0.08**	**0.12**	0.09	10.5	3.6	0.9	1.4	0.1
	D	dark green	**54.0**	**92.6**	**4.3**	**7.3**	**0.05**	**0.08**	0.06	9.3	4.9	0.6	0.5	0.2
	E	red	**64.6**	**83.6**	**12.6**	**16.3**	**0.10**	**0.13**	0.30	5.7	2.7	1.3	1.1	0.2
	Mean			**89.3**		**10.6**		**0.10**						
	SD			**4.7**		**4.6**		**0.04**						
P.624	A	dark green	**65.0**	**87.9**	**8.3**	**11.2**	**0.56**	**0.76**	0.69	5.4	3.6	2.7	3.5	0.3
	B	green	**58.4**	**86.5**	**8.6**	**12.8**	**0.44**	**0.65**	0.36	4.4	7.2	2.6	2.1	0.1
	C	green	**55.4**	**86.9**	**7.9**	**12.4**	**0.43**	**0.67**	0.26	4.4	4.7	1.7	1.8	0.1
	Mean			**87.1**		**12.2**		**0.70**						
	SD			**0.7**		**0.8**		**0.06**						

Tab.3. Results of the chemical composition using the "Patina" algorithm of the toilet spoons C.6428 and P.624 from the Museo Egizio (Turin). The chemical concentration is expressed in weigh percentage (wt%). Note: $Cu_{(N)}$, $Sn_{(N)}$ and $Pb_{(N)}$ are the normalized concentrations of the alloying elements; SD= Standard Deviation.

Artefact ID	Measuring point	Patina	Cu	Error (±)	Sn	Error (±)	Pb	Error (±)
C.6428	A	green	**94.2**	0.1	**5.78**	0.07	**0.04**	0.01
	B	grey	**86.6**	0.1	**13.33**	0.08	**0.12**	0.02
	C	green	**92.3**	0.1	**7.59**	0.06	**0.17**	0.02
	D	dark green	**92.5**	0.1	**7.38**	0.07	**0.14**	0.02
	E	red	**85.2**	0.1	**14.64**	0.08	**0.17**	0.02
	Mean		**90.1**		**9.74**		**0.13**	
	SD		**4.0**		**3.96**		**0.05**	
P.624	A	dark green	**88.7**	0.1	**10.14**	0.07	**1.12**	0.04
	B	green	**86.7**	0.1	**12.45**	0.09	**0.90**	0.05
	C	green	**87.7**	0.1	**11.41**	0.08	**0.93**	0.04
	Mean		**87.7**		**11.33**		**0.98**	
	SD		**1.0**		**1.16**		**0.12**	

Tab.4. Results of the chemical composition using the "Patina" algorithm of the toilet spoons C.6428 and P.624 from the Museo Egizio (Turin). The chemical concentration is expressed in weigh percentage (wt%). Note: $Cu_{(N)}$, $Sn_{(N)}$ and $Pb_{(N)}$ are the normalized concentrations of the alloying elements; SD= Standard Deviation; Error = algorithm error.